so that (28.1) is linearized to

$$\left(1-\frac{U^2}{c^2}\right)\varphi_{xx}+\varphi_{zz}+\frac{(U+\varphi_x)\,h_x}{h}+\frac{\varphi_z\,h_z}{h}=0, \tag{29.3}$$

$$c^2=g\,h(x,z). \tag{29.4}$$

In agreement with the previous discussion, (29.3) corresponds to the linearized gas dynamics equation only if the bottom is flat and horizontal, i.e. if h is constant.

The second method of linearization corresponds to the classical tidal-wave theory, or long-wave theory [see, e.g., LAMB (1932, p. 254) or Eqs. (10.36)] and can be obtained by writing

$$u(x,z,t)=\Phi_x\ll 1, \qquad w(x,z,t)=\Phi_z\ll 1, \tag{29.5}$$

$$\eta(x,z,t)\ll h(x,z), \tag{29.6}$$

so that (28.1) is linearized to

$$(\Phi_{xx}+\Phi_{zz})+\left(\frac{h_x}{h}\Phi_x+\frac{h_z}{h}\Phi_z\right)=\frac{1}{g\,h}\Phi_{tt}. \tag{29.7}$$

Again, as before, (29.7) corresponds to the linearized gas dynamic case, or the simple acoustic wave-propagation equation, only if the bottom is flat and horizontal. In this case the general solution of (29.7) for one-dimensional flow is the well known d'Alembert solution of the simple wave equation,

$$\Phi(x,t)=F(x-c\,t)+f(x+c\,t) \qquad c=\sqrt{g\,h}=\text{const}, \tag{29.8}$$

which is used to study long-wave-length oscillations in canals when the water is either at rest or moving with a velocity $U\ll c$. The limitation to small perturbations and constant h for one-dimensional flow allows (28.1) to be linearized to

$$\left.\begin{aligned}\Phi_{xt}&=u_t=-g\,\eta_x,\\ \eta_{xx}&=\frac{1}{g\,h}\eta_{tt}=\frac{1}{c^2}\eta_{tt};\end{aligned}\right\} \tag{29.9}$$

various applications of this, including the canal theory of tides, are given in LAMB (1932, pp. 254—273) and DEFANT (1957).

For the case of a canal having a non-rectangular but constant cross-section, we may generalize (29.9) by defining the mean depth h as the undisturbed cross-sectional area S divided by the width b of the canal at the undisturbed free water surface [see LAMB (1932), p. 256]. When the canal has a variable depth $h(x)$ and the disturbance may be considered one-dimensional, then (29.7) may be written in terms of the varying cross-sectional area $S(x)$ for constant width b as follows

$$\frac{1}{g\,h}\Phi_{tt}=\frac{1}{h}(h\,\Phi_x)_x=\frac{1}{S}(S\,\Phi_x)_x, \qquad S(x)=b\,h(x), \qquad b=\text{const}. \tag{29.10}$$

Then from (29.9) we obtain

$$\frac{1}{S}(S\,\eta_x)_x=\frac{1}{g\,h}\eta_{tt}, \tag{29.11}$$

which is the same as the expression derived by GREEN (1838) for a canal that is varying in both width b and depth h so that

$$S(x)=h(x)\,b(x).$$

However, the exact linearized first order approximation is (29.7), and the form of this equation indicates that large values of $b'(x)$ would invalidate the one-dimensional assumption, especially if h_z is relatively large. This is also indicated by LAMB (1932, p. 274). However, (29.7) provides the rigorous proof that (29.10) is applicable to one-dimensional, long-wavelength, small-amplitude disturbances in a canal of rectangular cross-section having a constant width and a varying depth.

If we now limit our analysis to long wave lengths having a simple harmonic oscillation of frequency $\sigma/2\pi$, so that we may write

$$\eta(x, t) = \eta(x) \sin(\sigma t + \tau), \qquad \Phi(x, t) = \varphi(x) \cos(\sigma t + \tau),$$

Eqs. (29.10) and (29.11) reduce to

$$\frac{1}{S}(S\varphi_x)_x + \frac{\sigma^2}{g h}\varphi = 0, \qquad \frac{1}{S}(S\eta_x)_x + \frac{\sigma^2}{g h}\eta = 0. \tag{29.12}$$

If we solve these equations in order to determine the harmonic oscillations in long canals with various special choices of varying cross-section, boundary conditions at the ends of the canal or finiteness conditions may further limit the allowable values of the frequency to a sequence of eigenvalues or fundamental frequencies, $\sigma_1, \sigma_2, \ldots$. Associated with each σ_i there is an η_i and Φ_i. The general solution of the Eqs. (29.12) is then a superposition of these characteristic solutions,

$$\eta(x, t) = \sum A_n \eta_n(x) \sin(\sigma_n t + \tau_n), \qquad \Phi(x, t) = \sum A_n \varphi_n(x) \cos(\sigma_n t + \tau_n),$$

where A_n and τ_n are arbitrary. Emphasis, however, is usually upon finding the fundamental mode σ_0, η_0 and the first few higher modes. We consider two special problems in order to illustrate the procedure. Other more complex situations are analyzed in LAMB (1932, p. 275 ff.) or in DEFANT (1957).

Let the canal be of rectangular cross-section with $h = h_0$, $b = \beta x$. We shall suppose it to be bounded at the ends by vertical walls at $x = x_1 > 0$, $x = x_2 > x_1$. The Eq. (29.12) for φ now becomes

$$\varphi_{xx} + \frac{1}{x}\varphi_x + \frac{\sigma^2}{g h}\varphi = 0,$$

BESSEL'S equation of order zero. The general solution is of the form

$$c\, J_0(\sigma x/c) + D\, Y_0(\sigma x/c), \qquad c^2 = g h.$$

The boundary conditions at the ends, $\phi'(x_1) = \phi'(x_2) = 0$, can be satisfied only if

$$J_1(\sigma x_1/c)\, Y_1(\sigma x_2/c) - J_1(\sigma x_2/c)\, Y_1(\sigma x_1/c) = 0.$$

This equation determines the eigenvalues $\sigma_1, \sigma_2, \ldots$. The various modes of motion are then of the form

$$\left.\begin{aligned} \Phi_n = A_n [Y_1(\sigma_n x_2/c)\, J_0(\sigma_n x/c) - J_1(\sigma_n x_2/c)\, Y_0(\sigma_n x/c)] \cos(\sigma_n t + \tau_n), \\ n = 1, 2, \ldots . \end{aligned}\right\} \tag{29.13}$$

If $x_1 = 0$, the solution Y_0 must be excluded because of its singularity at the origin and the eigenvalues are determined simply from $J_1(\sigma_n x_2/c) = 0$, $n = 1, 2, \ldots$.

A solvable case in which h is variable is the canal of rectangular cross-section with $b = b_0$ and

$$h(x) = h_0\left(1 - \frac{x^2}{L^2}\right).$$

Eq. (29.12) now becomes

$$\left(1 - \frac{x^2}{L^2}\right)\varphi_{xx} - 2\frac{x}{L^2}\varphi_x + \frac{\sigma^2}{g h_0}\varphi = 0, \tag{29.14}$$

the equation for the spherical harmonics $P_\nu(x/L)$, $Q_\nu(x/L)$ with $(\sigma L)^2/g h_0 = \nu(\nu+1)$. The condition that the solution should be finite on $|x| \leqq L$ requires one to discard Q_ν and further restricts ν to integers, thus determining the fundamental frequencies:

$$\sigma_n^2 = \frac{g h_0}{L^2} n(n+1).$$

The fundamental solutions are then formed with Legendre polynomials:

$$\Phi_n = A_n P_n(x/L) \cos(\sigma_n t + \tau_n). \tag{29.15}$$

Motions of the type considered above may be identified with the long period oscillations called seiches which occur in certain lakes or canals throughout the world. Many applications are presented by CHRYSTAL (1905, 1906) and the periods observed in several lochs and lakes seem to correspond to those calculated by the linear shallow-water theory. The linear shallow-water equation (29.7) should be very suitable for the study of seiches because of their long period and relatively small amplitude. Usually the complete Eq. (29.7) must be solved numerically by the method of finite differences because the contour of the body of water is quite irregular and the depth variation is important.

When the motion cannot be considered one-dimensional, one must use the complete two-dimensional equations (29.7). If the motion is harmonic with frequency $\sigma/2\pi$, so that

$$\eta(x, z, t) = \eta(x, z) \sin(\sigma t + \tau), \quad \Phi(x, z, t) = \varphi(x, z) \cos(\sigma t + \tau),$$

then the right-hand side of (29.7) is replaced by $-(\sigma^2/g h)\Phi$. However, just as in the one-dimensional case, the allowable values of σ may be restricted by the boundary conditions or finiteness conditions to a sequence of eigenvalues σ_1, $\sigma_2, \ldots$ with associated functions $\eta_1, \eta_2, \ldots, \Phi_1, \Phi_2, \ldots$. The general solution is again a superposition. We illustrate with several typical examples, but refer again to LAMB (1932, p. 282ff.) or DEFANT (1957) for a more comprehensive treatment.

Consider first a rectangular basin of constant depth h bounded by $x=0$, $x=x_0$, $z=0$, $z=z_0$. Then (29.7) becomes

$$\Phi_{xx} + \Phi_{zz} + \frac{\sigma^2}{g h}\Phi = 0$$

and the boundary conditions are

$$\Phi_x(0, z, t) = \Phi_x(x_0, z, t) = \Phi_z(x, 0, t) = \Phi_z(x, z_0, t) = 0.$$

It is easy to verify that the fundamental solutions are

$$\Phi_{mn} = A_{mn} \cos\frac{m\pi x}{x_0} \cos\frac{n\pi z}{z_0} \cos(\sigma_{mn} t + \tau_{mn}) \tag{29.16}$$

where the eigenvalues σ_{mn} are given by

$$\sigma_{mn} = \pi\sqrt{g h}\sqrt{\left(\frac{m}{x_0}\right)^2 + \left(\frac{n}{z_0}\right)^2}.$$

The result should be compared with (23.14) which reduces to this when $m_0 h$ is small enough so that $\tanh m_0 h \cong m_0 h$.

As another example consider a basin of circular planform of radius a and depth h. In polar coordinates, $x = r\cos\vartheta$, $y = r\sin\vartheta$, Eq. (29.7) becomes

$$\Phi_{rr} + \frac{1}{r}\Phi_r + \frac{1}{r^2}\Phi_{\vartheta\vartheta} + \frac{\sigma^2}{g h}\Phi = 0$$

and Φ must satisfy $\Phi_r(a, \vartheta, t) = 0$. The fundamental solutions are easily found by separation of variables to be

$$\Phi_{mn} = A_{mn} J_n(\sigma_{mn} r/c)\cos(n\vartheta + \delta_{mn})\cos(\sigma_{mn} t + \tau_{mn}), \qquad c^2 = g h, \tag{29.17}$$

where the fundamental frequencies σ_{mn} are the roots of

$$J_n'(\sigma_{mn} a/c) = 0, \qquad m = 1, 2, \ldots .$$

The solution (23.15) again reduces to this if $\tanh m_0 h \cong m_0 h$.

If the planform is ring-shaped with the rings having radii a and $b < a$, then one needs also the solution Y_n in order to satisfy the boundary condition on $r = b$. (The singularity of Y_n at the origin obviously causes no difficulty, for it is not in the fluid). The fundamental solutions now become

$$\left.\begin{aligned}\Phi_{mn} = A_{mn}\left[Y_n'\left(\frac{\sigma_{mn}}{c}b\right)J_n\left(\frac{\sigma_{mn}}{c}r\right) - J_n'\left(\frac{\sigma_{mn}}{c}b\right)Y_n\left(\frac{\sigma_{mn}}{c}r\right)\right]\times \\ \times\cos(n\vartheta + \delta_{mn})\cos(\sigma_{mn} t + \tau_{mn}),\end{aligned}\right\} \tag{29.18}$$

where the fundamental frequencies σ_{mn} are determined from the equation

$$J_n'\left(\frac{\sigma a}{c}\right)Y_n'\left(\frac{\sigma b}{c}\right) - J_n'\left(\frac{\sigma b}{c}\right)Y_n'\left(\frac{\sigma a}{c}\right) = 0. \tag{29.19}$$

As before, the solution (23.16) reduces to this one for small $m_0 h$.

As a final example of two-dimensional seiches we consider the long-period simple harmonic oscillation in a shallow circular basin with depth variation depending only on r. Then, in polar coordinates (29.7) becomes

$$\Phi_{rr} + \frac{1}{r}\Phi_r + \frac{1}{r^2}\Phi_{\vartheta\vartheta} + \frac{h_r}{h}\Phi_r + \frac{\sigma^2}{g h}\Phi = 0. \tag{29.20}$$

If the depth variation is parabolic,

$$h(r) = h_0\left(1 - \frac{r^2}{a^2}\right),$$

LAMB (1932, p. 291) has shown that the fundamental solutions are given by

$$\Phi_{mn} = A_{mn}\left(\frac{r}{a}\right)^m \cos(m\vartheta + \delta_{mn})\, F\left(\alpha, \beta, \gamma; \frac{r^2}{a^2}\right)\cos(\sigma_{mn} t + \tau_{mn}), \tag{29.21}$$

where F is the hypergeometric series

$$F\left(\alpha, \beta, \gamma; \frac{r}{a}\right) = 1 + \frac{\alpha\beta}{1\cdot\gamma}\left(\frac{r}{a}\right)^2 + \frac{\alpha(\alpha+1)\beta(\beta+1)}{1\cdot 2\cdot\gamma(\gamma+1)}\left(\frac{r}{a}\right)^4 + \cdots,$$

and

$$\alpha = m + n, \qquad \beta = 1 - n, \qquad \gamma = m + 1.$$

The fundamental frequencies σ_{mn} are determined from

$$\frac{\sigma_{mn}^2 a^2}{g h_0} = 2m(2n - 1) + 4n(n - 1).$$

Both m and n must be integers in the above formulas. They simplify in an obvious fashion for the symmetric mode $m=0$.

It has been pointed out above in connection with several of the examples that the results obtained by analyzing the problem by means of the infinitesimal-wave approximation reduce to those obtained by the linearized shallow-water approximation if $mh=2\pi h/\lambda$ is small enough so that $\tanh mh \cong mh$. One should note that this holds also for the velocity of propagation of a periodic wave:

$$c=\sqrt{\frac{g\lambda}{2\pi}\tanh\frac{2\pi h}{\lambda}}=\sqrt{gh}\left[1-\frac{1}{6}\left(\frac{2\pi h}{\lambda}\right)^2+\cdots\right]=\sqrt{gh}\left[1+O\left(\frac{h}{\lambda}\right)^2\right]. \quad (29.22)$$

The remainder $O(h/\lambda)^2$ confirms the appropriateness of the term "long-wave approximation" sometimes applied to the shallow-water theory.

This exact agreement of the linearized results in the limiting case is encouraging justification for both the shallow-water approximation and the infinitesimal-wave approximation since they originate not only from different physical considerations, but also by entirely different types of mathematical approximation, as discussed in Sect. 10. The shallow-water approximation leads to hyperbolic type nonlinear equations, while the infinitesimal-wave approximation deals with linear elliptic equations. STOKER (1947, p. 32) gives a detailed comparison of the two linearized approximations for the case of wave motion over a flat bottom at a 6° slope.

α) *Linearized shallow-water theory applied to two-dimensional steady flow.* The first method of linearizing the shallow-water theory, as given by (29.3), is applicable to the determination of the variation in water depth for the steady flow in a shallow open channel or river. However, in practically all cases (29.3) must be solved numerically, so that it does not entail a prohibitive amount of extra labor to solve directly the more exact original nonlinear first-order equations (28.1) using the methods discussed in the next section (30) on nonlinear first-order theory. As a matter of fact, for supercritical flow, defined by $U>\sqrt{gh}$, the method of characteristics is very easy to use in the numerical solution for a nearly horizontal open channel having a flat bottom and varying width, as shown in Sect. 30. The subcritical case, having a flow velocity everywhere less than $\sqrt{gh}$, can be satisfactorily approximated by the one-dimensional hydraulic theory which assumes that the velocity at each cross-section $S(x)$ is independent of y and z. This method would yield, of course, a constant depth over a given cross-section and would therefore not be satisfactory for predicting the rise in water level about an island, or a jetty, or a pile in a swiftly moving relatively wide stream. For this particular application the linearized form of (29.3) is very useful, especially for subcritical flow, i.e. for $U^2/gh<1$.

We now consider the application of (29.3) to the problem of determining the water depth variation about a two-dimensional cylinder that is perpendicular to the bottom and has a narrow cross-section parallel to the flow as shown in Fig. 37. If the bottom is approximately flat and horizontal everywhere near the vertical cylinder, then we may consider h as constant and, providing that $U^2/gh<1$, write (29.3) as

$$\left.\begin{aligned}\beta^2\varphi_{xx}+\varphi_{zz}=0 \quad \text{or} \quad \frac{\partial^2\varphi}{\partial x^2}+\frac{\partial^2\varphi}{\partial(\beta z)^2}=0,\\ \beta^2=1-F^2=1-\frac{U^2}{gh}=\text{const}>0.\end{aligned}\right\} \quad (29.23)$$

The fundamental solution of (29.23), in view of (29.1), for two-dimensional profiles which may be considered symmetrical about the z-axis as shown in Fig. 37, is

$$\left.\begin{aligned} \varphi(x,z) &= +\frac{1}{2\pi}\int_0^L f(\xi)\ln\sqrt{(x-\xi)^2+(\beta z)^2}\,d\xi, \\ u &= U+\varphi_x = U+\frac{1}{2\pi}\int_0^L \frac{(x-\xi)\,f(\xi)\,d\xi}{(x-\xi)^2+(\beta z)^2}, \\ w &= \varphi_z = \frac{\beta^2 z}{2\pi}\int_0^L \frac{f(\xi)\,d\xi}{(x-\xi)^2+(\beta z)^2}. \end{aligned}\right\} \tag{29.24}$$

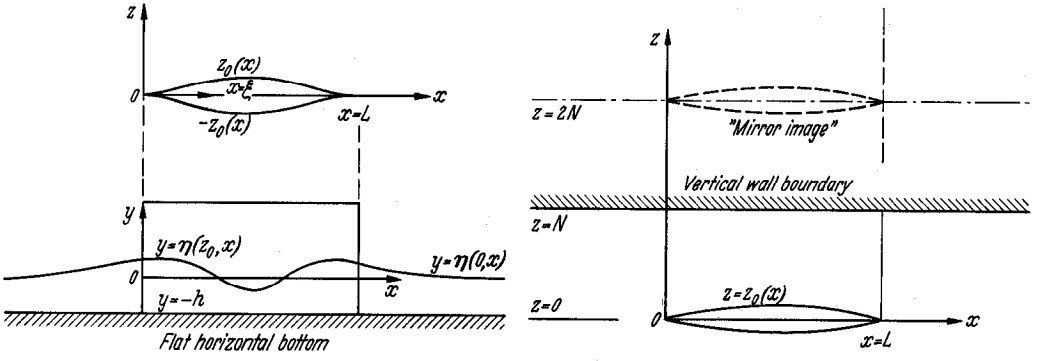

Fig. 37. Shallow-water flow about a two-dimensional symmetrical cylinder perpendicular to the flat horizontal bottom.

The boundary condition for the two-dimensional shape (see Fig. 37) is

$$\frac{dz_0}{dx}=\frac{w}{u}=\frac{\varphi_z(x,z_0)}{U+\varphi_x(x,z_0)}=\frac{\varphi_z}{U}\left[1+O\left(\frac{\varphi_x}{U}\right)\right], \tag{29.25}$$

where the same linearization procedure has been applied to the boundary condition as was used in deriving (29.3). Therefore (29.24) may also be similarly linearized by writing

$$U\frac{dz_0}{dx}=\varphi_z(x,z_0)=\frac{\beta}{2\pi}\int_0^L \frac{f(\xi)\left(\frac{d\xi}{\beta z_0}\right)}{1+\left(\frac{x-\xi}{\beta z_0}\right)^2}.$$

Hence if we let $\frac{(x-\xi)}{\beta z_0}=p$, then for $z_0\leqq 0$,

$$U\frac{dz_0}{dx}=\frac{\beta}{2\pi}\int_{-\frac{L-x}{\beta z_0}}^{\frac{x}{\beta z_0}} \frac{f(x-\beta z_0 p)\,dp}{1+p^2}=\frac{1}{2}\beta f(x)+O(z_0^2).$$

Therefore

$$f(\xi)=\frac{2U}{\beta}z_0'(\xi)+O(z_0^2), \tag{29.26}$$

so that the linearized form of (29.24) is

$$\left.\begin{aligned} \frac{u(x,z)}{U} &= 1+\frac{1}{\pi\beta}\int_0^L \frac{(x-\xi)\,z_0'(\xi)\,d\xi}{(x-\xi)^2+(\beta z)^2}=1+\frac{\varphi_x}{U}, \\ \frac{w(x,z)}{U} &= \frac{z\beta}{\pi}\int_0^L \frac{z_0'(\xi)\,d\xi}{(x-\xi)^2+(\beta z)^2}=\frac{\varphi_z}{U}. \end{aligned}\right\} \tag{29.27}$$

On the actual surface of the two-dimensional profile (29.27) may be further linearized to

$$\left.\begin{aligned} \frac{u(x,z_0)}{U} &= 1+\frac{1}{\pi\beta}\left[\lim_{\varepsilon\to 0}\int_0^{x-\varepsilon}+\int_{x+\varepsilon}^{L}\frac{z_0'(\xi)\,d\xi}{x-\xi}\right]=1+\frac{1}{\pi\beta}\,\mathrm{PV}\int_0^L\frac{z_0'(\xi)}{x-\xi}\,d\xi,\\ \frac{w(x,z_0)}{U} &= z_0'(x). \end{aligned}\right\} \tag{29.28}$$

On the other hand, for large values of z we may write

$$\frac{u(x,z)}{U}\approx 1+\frac{1}{\pi\beta^3 z^2}\int_0^L(x-\xi)\,z_0'(\xi)\,d\xi,\qquad \frac{w(x,z)}{U}\approx\frac{1}{\pi\beta z}\int_0^L z_0'(\xi)\,d\xi. \tag{29.29}$$

The change $\eta(x,z)$ in the original constant water depth h can then be determined by the linearized relations corresponding to (29.1) and (29.2) as

$$\frac{\eta(x,z)}{h}+O\left(\frac{\eta}{h}\right)^2=-F^2\frac{\varphi_x}{U}+O\left(\frac{\varphi_x^2+\varphi_z^2}{U^2}\right),\qquad F^2=\frac{U^2}{gh}, \tag{29.30}$$

where for any (x,z) we obtain φ_x and φ_z from (29.27). For example, on the surface of the two-dimensional profile $(z=z_0)$, (29.30) reduces to

$$\frac{\eta(x,z_0)}{h}=-\frac{U^2}{gh}\frac{1}{\pi\beta}\left[\mathrm{PV}\int_0^L\frac{z_0'(\xi)\,d\xi}{x-\xi}+O(z_0^2)\right] \tag{29.31}$$

where φ_x and φ_z are both of $O(z_0')$.

These relations are, of course, completely restricted to flows that are everywhere subcritical since (29.23) shows that the Froude number $(F=U/\sqrt{gh})$ must be everywhere less than unity to keep $\beta>0$. The effect of increasing Froude number is to increase φ_x, and therefore decrease η, since β decreases. It is seen that this effect increases as z increases, the greatest effect being on $\varphi_x\sim 1/\beta^3$ in the limiting case of very large values of z as shown in (29.29). This relation, or preferably (29.27), could be used to predict the additional change in $\eta(x,z)$ due to a finite stream width by using the increment of φ_x from one mirror image to represent the first approximation to the channel boundary wall as indicated in Fig. 37. For slender cylinders in a narrow channel the "one-dimensional" approximation of Sect. 30γ is generally used, this allows an approximation for frictional head loss which becomes relatively more important as the channel width decreases.

For supercritical flow $(F=U/\sqrt{gh}>1)$, (29.23) must be written as

$$\left.\begin{aligned} &B^2\varphi_{xx}-\varphi_{zz}=0\quad\text{or}\quad\frac{\partial^2\varphi}{\partial x^2}=\frac{\partial^2\varphi}{\partial(Bz)^2},\\ &B^2=F^2-1=\frac{U^2}{gh}-1=\text{const}>0. \end{aligned}\right\} \tag{29.32}$$

Now, however, (29.32) cannot provide a satisfactory approximation of the change in water depth at some distance from the two-dimensional profile since its general solution is

$$\varphi(x,z)=G(x-Bz)+g(x+Bz), \tag{29.33}$$

which predicts no change, even upon approaching infinity, along the lines of constant slope $dz/dx=\pm 1/B=\pm[F^2-1]^{-\frac{1}{2}}$. Consequently the nonlinear method

of characteristics, which will be described in Sect. 30, must be used in predicting the depth variation at any finite distance from the profile. Although the method of characteristics will directly and easily give the velocity distribution or depth variation on the profile itself, we will also derive the variation on the profile surface according to the linearized theory. The result will be of crucial importance in evaluating the validity of the nonlinear first-order shallow-water theory (28.1), since any great discrepancy between the linearized result and the nonlinear results from (28.1) would indicate that the perturbations involved are sufficiently large that the second-order shallow-water theory of Sect. 31 must be introduced.

The linearized solution of (29.32) for any sharp-nosed slender two-dimensional profile, as in Fig. 37, is obtained from the general solution (29.33) and the following linearized boundary condition:

$$z_0'(x) = \frac{\varphi_z(x, z_0)}{U} = -\frac{B}{U} G'(x - B z_0); \qquad z = z_0 > 0.$$

Therefore $G'(x - B z_0) = -U z_0'(x)/B$, so that on the profile surface, $z = z_0(x)$,

$$\left.\begin{aligned} u(x, z_0) &= U + \varphi_x = U + G'(x - B z_0) = U\left[1 - \frac{z_0'(x)}{B}\right], \\ w(x, z_0) &= U z_0'(x). \end{aligned}\right\} \tag{29.34}$$

Then the variation in water depth on the profile surface is given by (29.30) as

$$\frac{\eta(x, z_0)}{h} = F^2\left[\frac{z_0'(x)}{B} + O(z_0'^2)\right] \tag{29.35}$$

for flow that is everywhere supercritical, i.e. $B^2 = F^2 - 1 > 0$.

It should be noted that (29.23) and (29.32) are identical to the linearized potential equations for two-dimensional steady subsonic flow and supersonic flow, respectively, if we simply replace the Froude number ($F = U/\sqrt{gh}$) by the Mach number ($M = U/c$) [see (28.3)]. This is in complete accord with the statement that the hydraulic analogy is valid for the flow over a flat horizontal bottom (i.e., the flow is equivalent to the two-dimensional isentropic flow of a fictitous perfect gas having a specific heat ratio $\gamma = 2$). Consequently, Eqs. (29.24) through (29.29) are identical to these for subsonic flow about slender two-dimensional profiles in free air or in a wind tunnel of rectangular cross-section as derived by LAITONE (1946). These equations confirm the known result that the linearized equations are independent of the value of the specific heat ratio γ. Similarly, Eq. (29.34) is identical to the well-known linearized two-dimensional supersonic-flow solution if we let $F^2 - 1 \equiv B^2 = M^2 - 1 > 0$.

Although these linearized results are very satisfactory for slender sharp-nosed profiles, they only apply for Froude numbers that are not too near unity, that is they are not applicable to flows near the critical velocity $U = \sqrt{gh} = c$, equivalent to sonic flow. For these cases we must return to the nonlinear equation (28.1), as discussed in Sect. 30.

30. Nonlinear shallow-water theory. This section will primarily discuss methods for obtaining solutions of the nonlinear equations (28.1) which provide the first-order approximation of the shallow-water theory. The special cases to be considered are the one-dimensional unsteady flow and the two-dimensional steady flow in open channels. This will provide a basis for discussing the one-dimensional assumption of open-channel flow. Finally the hydraulic jumps, and their relation to the first-order shallow-water theory, will be discussed.

α) One-dimensional non-steady, first-order, shallow-water theory. By assuming one-dimensional flow in the x direction only, the nonlinear equations (28.1) reduce to

$$\left.\begin{aligned} u_t + u\,u_x + g(\eta + h)_x &= g\,h_x, \\ (\eta + h)_t + [u(\eta + h)]_x &= h_t = 0. \end{aligned}\right\} \tag{30.1}$$

Again it should be noted that these are equivalent to the gas dynamic equations, upon introducing (28.3), only if the bottom is flat and horizontal, i.e. $h_x = 0$.

Now, if we let

$$\left.\begin{aligned} c^2(x,t) &= g[\eta(x,t) + h(x)], \\ 2c\,c_x = g(\eta + h)_x, &\quad 2c\,c_t = g(\eta + h)_t, \end{aligned}\right\} \tag{30.2}$$

and give the initial conditions as $du/d\alpha$ and $dc/d\alpha$ along a curve in the (x, t)-plane defined by $x(\alpha)$, $t(\alpha)$, then we may write (30.1) as

$$\left.\begin{aligned} u\,u_x + u_t + 2c\,c_x + 0 &= g\,h_x, \\ c\,u_x + 0 + 2u\,c_x + 2c_t &= 0, \\ x_\alpha\,u_x + t_\alpha\,u_t + 0 + 0 &= \frac{du}{d\alpha}, \\ 0 + 0 + x_\alpha\,c_x + t_\alpha\,c_t &= \frac{dc}{d\alpha}, \end{aligned}\right\} \tag{30.3}$$

This set of four equations can be solved uniquely for u_x, u_t, c_x, c_t in terms of u, c, h_x and the initial conditions as long as the determinant of the coefficients in (30.3) does not vanish. This condition is violated along the characteristic curves $x(\alpha)$, $t(\alpha)$ defined by

$$\begin{vmatrix} u & 1 & 2c & 0 \\ c & 0 & 2u & 2 \\ x_\alpha & t_\alpha & 0 & 0 \\ 0 & 0 & x_\alpha & t_\alpha \end{vmatrix} = 0, \tag{30.4}$$

which may be easily expanded by the minors of the bottom row to give

$$x_\alpha^2 - 2u\,x_\alpha t_\alpha + (u^2 - c^2)\,t_\alpha^2 = [x_\alpha - (u - c)\,t_\alpha]\,[x_\alpha - (u + c)\,t_\alpha] = 0.$$

Therefore the characteristic curves, C_+ and C_-, are defined by

$$\frac{x_\alpha}{t_\alpha} = \left(\frac{dx}{dt}\right)_{C_\pm} = u(x,t) \pm c(x,t). \tag{30.5}$$

Since h_x is given, and appears only on the right-hand side of the first equation in (30.3), therefore the characteristic curves as defined in (30.5) are identical to those in the gas-dynamics case [see, e.g., COURANT and FRIEDRICHS (1948)]. However, the Riemann invariants, or quantities that can be constant along a characteristic curve, now depend upon the bottom slope, as may be seen by adding the two equations in (30.1) after introducing (30.2) so as to obtain

$$(u + 2c)_t + (u + c)\,(u + 2c)_x = \left[\frac{\partial}{\partial t} + (u + c)\,\frac{\partial}{\partial x}\right][u(x,t) + 2c(x,t)] = g\,h_x. \tag{30.6}$$

These give the same Riemann invariants as in the isentropic one-dimensional unsteady gas flow with a specific heat ratio $\gamma = 2$ only if $h_x = 0$ [see, e.g.,

COURANT and FRIEDRICHS (1948, p. 87)]. No simple Riemann invariant involving only u and c is possible if h_x varies with x; however, if h_x is constant, so that $gh_x = m = \text{const}$, then (30.6) may be written

$$\left[\frac{\partial}{\partial t} + (u+c)\frac{\partial}{\partial x}\right][u + 2c - mt] = 0. \tag{30.7}$$

Similarly, by subtracting the two equations in (30.1), we obtain

$$\left[\frac{\partial}{\partial t} + (u-c)\frac{\partial}{\partial x}\right][u - 2c - mt] = 0. \tag{30.8}$$

Consequently, the basic statements relating the characteristic curves and Riemann invariants of Eq. (30.1) with $gh_x = m = \text{const}$ may be summarized as follows:

$$\left.\begin{aligned} u + 2c - mt = R(x,t) &= \text{const along a curve } C_+ \\ &\text{defined by } \frac{dx}{dt} = u + c; \\ u - 2c - mt = -S(x,t) &= \text{const along a curve } C_- \\ &\text{defined by } \frac{dx}{dt} = u - c. \end{aligned}\right\} \tag{30.9}$$

Fig. 38 shows typical sets of curves in the (x, t)-plane. The above equations show that in any given region in the (x, t)-plane there are three basic types of solutions, namely:

(1) the constant steady state in which u and c remain constant everywhere in the region, so that all characteristics form straight lines;

(2) the general flow in which neither R nor S is constant in a finite region;

(3) the special case of a simple wave over a flat horizontal bottom ($m = 0$) wherein a constant steady-state region is separated from a varying region by a straight characteristic line along which either R or S is constant.

The first type of solution obviously has R and S constant throughout the region only if the bottom is flat and horizontal ($m = 0$). The second type of solution is complicated and can best be obtained by the method of finite differences [see, e.g., STOKER (1957, pp. 293–300)]. The third type of solution will now be discussed since it has considerable physical significance for many problems concerning the propagation of a disturbance into water that is originally at constant depth and constant velocity, and extends an unlimited distance for $x > 0$.

When a disturbance moves into still water at constant depth over a flat horizontal bottom ($m = 0$), then it is obvious that $(dx/dt)_0 = c(\infty)$ is the characteristic, now a straight line, which must continually separate the steady-state region from the disturbance region in the (x, t)-plane, as indicated in Fig. 38. This characteristic curve must be a straight line since there is a constant steady state always ahead of it so that $(dx/dt)_0 = \text{const}$ and therefore $x_0 = c(\infty)\, t$. Also, either R or S must be constant along the characteristic, and since R_0 corresponds to C_+^0 or $(dx/dt)_0 = c(\infty) > 0$, as in Fig. 38, therefore $R_0 = 2c(\infty) = \text{const}$. This type of simple wave, having $(dx/dt)_0 = c(\infty) > 0$ and $R_0 = 2c(\infty) = \text{const.}$, is called a forward-facing wave since the particle paths enter from the side with greater values of x, as in Fig. 38. The value of R varies as one passes from one to another C_+ characteristic inside the region of the disturbance since u and c both vary due to the disturbance and none of the C_+ characteristic lines can ever

intersect C_+^0. However, every C_- characteristic intersects C_+^0, as shown in Fig. 38, and since S remains constant on any given C_- characteristic curve, therefore S is everywhere constant since every C_- characteristic must have the same value $S(x,t) = R_0 = 2c(\infty) = \text{const}$ on C_+^0.

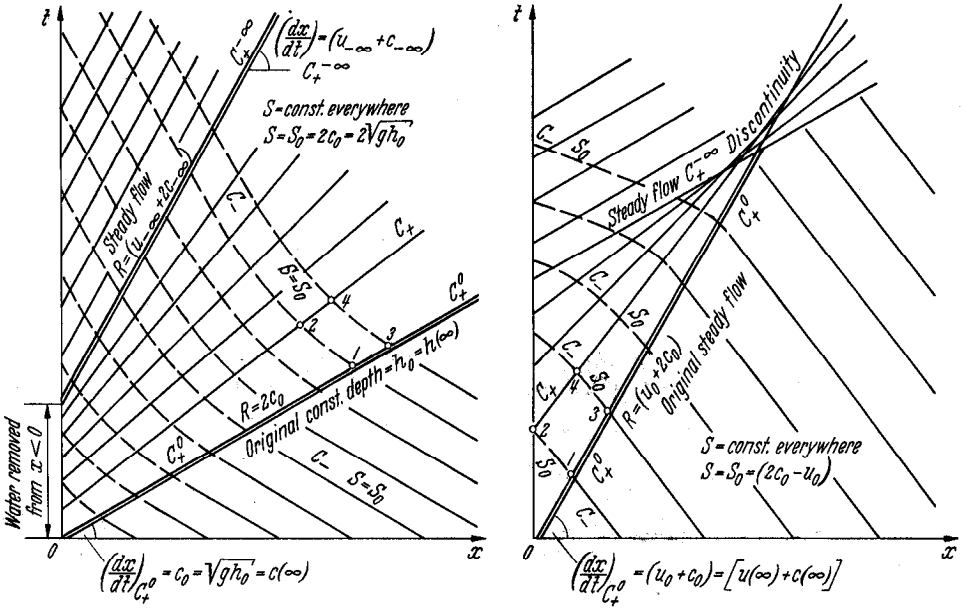

Fig. 38. Simple forward-facing waves, $S = \text{const}$.

The same considerations are true even if the water of constant depth into which the disturbance is being propagated is flowing with a constant velocity $u(\infty) < c(\infty)$. The only change is that now the following are constant:

$$\left(\frac{dx}{dt}\right)_0 = u(\infty) + c(\infty) > 0, \qquad R_0 = 2c(\infty) + u(\infty)$$

on C_+^0 only, while on all C_-,

$$2c(x,t) - u(x,t) = S(x,t) = 2c(\infty) - u(\infty) = \text{const}.$$

Similarly all R in the disturbance region vary as

$$R(x,t) = 2c(x,t) + u(x,t),$$

as indicated in Fig. 38 for the simple forward-facing (C_+^0) wave. As shown in Fig. 39 a simple backward-facing (C_-^0) occurs if $R = \text{const}$ and $S = 2c - u$. These waves are called simple waves because all the characteristics of the family for which the Riemann invariant takes on a different constant for each line form straight lines. For example, referring to Fig. 38, the forward-facing waves ($dx/dt > 0$) have $S(x,t)$ constant everywhere and $R(x,t)$ varying so that the C_+ characteristics form straight lines. On the other hand, in Fig. 39 the backward-facing wave ($dx/dt < 0$) has $R(x,t)$ constant everywhere and $S(x,t)$ varying, so that now only the C_- characteristics form straight lines. The characteristics of one family only must form straight lines in a simple wave because only one of the Riemann invariants (S or R) is constant in the entire region of the disturbance. For example, in the case of the forward-facing simple wave in Fig. 38,

we have S constant in the region of the disturbance. Therefore from (30.9) and Fig. 38 we may write,

$$-S_1 = -S_2 = -S_3 = -S_4 = u_1 - 2c_1 = u_2 - 2c_2 = u_3 - 2c_3 = u_4 - 2c_4 = \text{const},$$

$$R_1 = R_3 = u_1 + 2c_1 = u_3 + 2c_3 \neq R_2 = R_4 = u_2 + 2c_2 = u_4 + 2c_4.$$

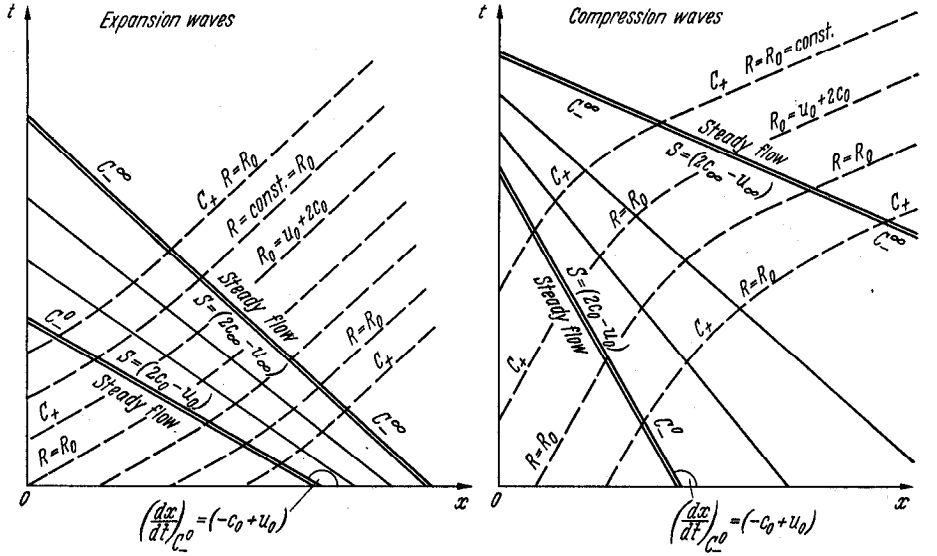

Fig. 39. Simple backward-facing waves, $R = \text{const.}$

Consequently, $u_1 = u_3$, $c_1 = c_3$, $u_2 = u_4$, $c_2 = c_4$, and $u_1 \neq u_2$, $c_1 \neq c_2$, $u_3 \neq u_4$, $c_3 \neq c_4$, so that

$$\left(\frac{dx}{dt}\right)_{C_-} = u_1 - c_1 \neq u_2 - c_2 \neq \text{const}, \qquad (C_- \text{ curved}),$$

$$\left(\frac{dx}{dt}\right)_{C_+^0} = u_1 + c_1 = u_3 + c_3 = \text{const}, \qquad (C_+^0 \text{ straight}),$$

$$\left(\frac{dx}{dt}\right)_{C_+} = u_2 + c_2 = u_4 + c_4 = \text{const}, \qquad (C_+ \text{ straight}).$$

It is important to note that these simple waves can exist only over a flat horizontal bottom, i.e. when $m = 0$.

We have now shown how the method of characteristics for one-dimensional unsteady flow has resulted in the concept of the simple wave which quickly gives a numerical evaluation of the propagation of a one-dimensional disturbance into water of constant depth moving at constant speed. The solution of this problem in the (x, t)-plane can be obtained by direct application of (30.9). For example, the usual case of a forward-facing wave having S everywhere constant, and straight C_+ characteristic lines, as shown in Fig. 38, has the slope of the C_+ straight lines determined directly by the time history of the disturbance at $x = 0$, and Eqs. (30.2) and (30.9) which show that

$$\left(\frac{dx}{dt}\right)_{C_+} = u(0, t) + c(0, t) = \text{const} = u(0, t) + \sqrt{g[h + \eta(0, t)]}. \qquad (30.10)$$

Along any given C_+ straight line having this constant slope

$$R(x, t)_{C_+} = u(0, t) + 2c(0, t) = \text{const} = u(0, t) + 2\sqrt{g[h + \eta(0, t)]}. \qquad (30.11)$$

Consequently, the values of u and c are determined in the entire region shown in Fig. 38 by the given values on the t-axis. The curved C_- characteristics need not be calculated, since the desired numerical solution is independent of them. Their existence, however, can lead to a simplification in the numerical calculation of (30.10) since, in the case shown in Fig. 38, each curved C_- characteristic extends from the C_+^0 characteristic to the t-axis, and on each and every C_- characteristic, $-S=u(\infty)-2c(\infty)=\text{const}$. Therefore, at every point on the t-axis that can be reached by a C_- characteristic we must have

$$S=2c(0,t)-u(0,t)=2c(\infty)-u(\infty)=2\sqrt{gh}-u(\infty)=\text{const}. \quad (30.12)$$

Of course the C_- characteristics can continue from C_+^0 to the t-axis only if $(dx/dt)_{C_-}=u-c<0$, or $u<c$, so that in this case (30.10) may be simplified to

$$\left.\begin{aligned}\left(\frac{dx}{dt}\right)_{C_+}&=u(0,t)+c(0,t)=\text{const}\\&=\tfrac{3}{2}u(0,t)-\tfrac{1}{2}[u(\infty)-2c(\infty)]=\tfrac{3}{2}u(0,t)-\tfrac{1}{2}u(\infty)+\sqrt{gh}\\&=3c(0,t)+[u(\infty)-2c(\infty)]=3\sqrt{g[h+\eta(0,t)]}+u(\infty)-2\sqrt{gh}.\end{aligned}\right\} \quad (30.13)$$

Consequently, the problem is solved in the region so defined if either $u(0,t)$ or $c(0,t)$ is alone given. The surface elevation is given by (30.2) as

$$h+\eta(x,t)=\frac{c^2(x,t)}{g}, \qquad h=\frac{c^2(\infty)}{g}=\text{const} \quad (30.14)$$

in every case of disturbance propagations into a constant water depth over a flat horizontal bottom ($m=0$).

Many other physical problems can be simulated by giving the data along a prescribed curve in the (x,t)-plane for $x\leqq 0$; e.g., see STOKER (1957) where the disturbance created by the breaking of a dam, and the effect of moving a vertical end plate in a tank of still water of rectangular cross-section, $u(\infty)=0$, are considered. Since the bottom is flat and horizontal ($m=0$), all of the equations following (30.9) are equivalent to the gas-dynamics equations with a specific heat ratio $\gamma=2$. Consequently, the problems solved in COURANT and FRIEDRICHS (1948) for channels of finite length which produce wave reflections at either end are also applicable. In this hydraulic analogy to compressible flow it is important to remember that (30.13) is only applicable to subcritical flow, which is equivalent to subsonic gas flow, since we must have $(dx/dt)_{C_-}=u-c<0$, or $u(\infty)<c(\infty)=\sqrt{gh}$. When the flow is supercritical, so that $u(\infty)>c(\infty)=\sqrt{gh}$, corresponding to supersonic gas flow, then the slopes of both the C_+ and C_- characteristics are positive. Consequently the two families can meet in a cusp, and the C_- characteristics cannot intersect both the t-axis and the undisturbed steady supercritical state that lies at, and to the right of, C_+^0. Therefore, in order to apply (30.13) for supercritical flow, the region of the constant value of S, as given by (30.12), must be very carefully defined.

Another limitation on all the preceding equations is indicated for the compression wave depicted in Figs. 38 and 39. This limitation is defined by the envelope of the straight characteristic lines that *must* always form for a compression wave in this first-order theory, as will be proven later. This envelope of the straight characteristic lines corresponds to a discontinuity that can be interpreted as a discontinuity in η, or the breaking of the wave crest. This leads to the hydraulic jump or surge that will be discussed later. The gas dynamic case has the envelope of the straight characteristic lines interpreted as a steady-state shock wave [see, e.g., COURANT and FRIEDRICHS (1948, pp. 110—181)].

β) Two-dimensional, steady, supercritical flow by the first-order shallow-water theory. We will now investigate the characteristic curves of the nonlinear equations of the first-order shallow-water theory for the case of steady two-dimensional flow. We will find that real characteristic curves, which are a great aid to numerical calculations, exist only in the regions wherein the flow is everywhere supercritical.

If we consider the steady two-dimensional flow over a flat horizontal bottom, then we may write (28.2) as

$$\left.\begin{aligned} &u\,u_x + w\,u_z = -\,g\,(\eta + h_0)_x = -\,(c^2)_x,\\ &u\,w_x + w\,w_z = -\,g\,(\eta + h_0)_z = -\,(c^2)_z,\\ &[u\,(\eta + h_0)]_x + [w\,(\eta + h_0)]_z = 0 \quad \text{or} \quad (u\,c^2)_x + (w\,c^2)_z = 0,\\ &u = \varphi_x, \quad w = \varphi_z, \quad u_z = w_x = \varphi_{xz}. \end{aligned}\right\} \tag{30.15}$$

By multiplying the first equation by $u = \varphi_x$ and the second by $w = \varphi_z$, and adding, we obtain

$$\varphi_x^2\,\varphi_{xx} + 2\,\varphi_x\,\varphi_z\,\varphi_{xz} + \varphi_z^2\,\varphi_{zz} = -\,[\varphi_x\,(c^2)_x + \varphi_z\,(c^2)_z] = (\varphi_{xx} + \varphi_{zz})\,c^2. \tag{30.16}$$

Therefore

$$\left(\frac{\varphi_x^2}{c^2} - 1\right)\varphi_{xx} + 2\,\frac{\varphi_x\,\varphi_z}{c^2}\,\varphi_{xz} + \left(\frac{\varphi_z^2}{c^2} - 1\right)\varphi_{zz} = 0 \tag{30.17}$$

or

$$\left(1 - \frac{u^2}{c^2}\right)\varphi_{xx} - 2\,\frac{u\,w}{c^2}\,\varphi_{xz} + \left(1 - \frac{w^2}{c^2}\right)\varphi_{zz} = 0 \tag{30.18}$$

where $c^2(x, z) = g[h_0 + \eta(x, z)]$ and h_0 now is the still water depth found whenever $(u^2 + w^2) = 0 = \eta$. Note that (30.18) immediately linearizes to (29.3), so that the numerical differences between the solutions of (29.3) and (30.18) will provide an estimate of whether or not the second-order shallow-water theory, as discussed in Sect. 31, must be introduced.

The characteristic curves of (30.18) may be found in a manner similar to that used for (30.3) by finding the curve $[x(\alpha), z(\alpha)]$ in the (x, z)-plane along which prescribed values of φ_x and φ_z cannot determine φ_{xx}, φ_{xz} and φ_{zz}. Therefore we write

$$\left.\begin{aligned} &\left(1 - \frac{u^2}{c^2}\right)\varphi_{xx} + \left(-\,2\,\frac{u\,w}{c^2}\right)\varphi_{xz} + \left(1 - \frac{w^2}{c^2}\right)\varphi_{zz} = 0,\\ &x_\alpha\,\varphi_{xx} + z_\alpha\,\varphi_{xz} + 0 = \frac{d\,\varphi_x}{d\alpha},\\ &0 + x_\alpha\,\varphi_{xz} + z_\alpha\,\varphi_{zz} = \frac{d\,\varphi_z}{d\alpha}, \end{aligned}\right\} \tag{30.19}$$

which may not have a solution if the determinant of the coefficient is zero, that is if

$$\begin{vmatrix} 1 - \dfrac{u^2}{c^2} & -\,\dfrac{2\,u\,w}{c^2} & 1 - \dfrac{w^2}{c^2} \\ x_\alpha & z_\alpha & 0 \\ 0 & x_\alpha & z_\alpha \end{vmatrix} = 0, \tag{30.20}$$

or

$$\left.\begin{aligned} &\left(1 - \frac{u^2}{c^2}\right)z_\alpha^2 + 2\,\frac{u\,w}{c^2}\,z_\alpha\,x_\alpha + \left(1 - \frac{w^2}{c^2}\right)x_\alpha^2 = 0,\\ &\frac{z_\alpha}{x_\alpha} = \left(\frac{dz}{dx}\right)_{C_\pm} = \frac{\dfrac{u\,w}{c^2} \pm \sqrt{\dfrac{u^2 + w^2}{c^2} - 1}}{\dfrac{u^2}{c^2} - 1} \end{aligned}\right\} \tag{30.21}$$

which therefore gives the slopes of the two families (C_+ and C_-) of characteristic curves. Now, however, entirely unlike the previous one-dimensional unsteady flow solution, the characteristic curves exist only for supercritical flow, i.e., for $u^2+w^2>c^2=g(h_0+\eta)$. The fact that the characteristic curves are real for supercritical flow means that in this case the nonlinear equation (30.17) is hyperbolic. However, for subcritical flow, since the characteristic curves are then complex functions, it is of elliptic type [see, e.g., COURANT and FRIEDRICHS (1948, pp. 40—55) or PREISWERK (1938)].

We can obtain a solution for the behavior of the quantity

$$F(x,z)=\sqrt{\frac{u^2+w^2}{c^2}}\geqq 1 \tag{30.22}$$

(which defines the Froude number of the supercritical flow) along a characteristic curve by transforming (30.18) into the (u, w)-plane, called the hodograph plane, through the use of the Legendre contact transformation which is given by [see, e.g., COURANT and FRIEDRICHS (1948, p. 249) or PREISWERK (1938)]

$$\chi=(x\varphi_x+z\varphi_z-\varphi)=(xu+zw-\varphi),$$
$$d\chi=(x\,du+u\,dx+z\,dw+w\,dz-d\varphi)=(x\,du+z\,dw).$$

Hence

see errata

$$x=\chi_u,\quad z=\chi_w,$$
$$dx=x_u\,du+x_w\,d_w=\chi_{uu}\,du+\chi_{uw}\,dw,$$
$$dy=z_u\,du+z_w\,dw=\chi_{uw}\,du+\chi_{ww}\,dw.$$

Solving for du and dw, we obtain

$$du=N^{-1}(\chi_{ww}\,dx-\chi_{uw}\,dz)=d\varphi_x=\varphi_{xx}\,dx+\varphi_{xz}\,dz,$$
$$dw=N^{-1}(-\chi_{uw}\,dx+\chi_{uu}\,dz)=d\varphi_z=\varphi_{xz}\,dx+\varphi_{zz}\,dz,$$

where

$$N=\begin{vmatrix}\chi_{uu} & \chi_{uw}\\ \chi_{uw} & \chi_{ww}\end{vmatrix}\neq 0,$$

so that

$$\varphi_{xx}=\frac{\chi_{ww}}{N},\qquad \varphi_{xz}=-\frac{\chi_{uw}}{N},\qquad \varphi_{zz}=\frac{\chi_{uu}}{N}.$$

The nonlinear equation (30.17) in the physical (x, z)-plane is transformed into the following linear equation in the hodograph (u, w)-plane:

$$\left(\frac{w^2}{c^2}-1\right)\chi_{uu}-2\frac{uw}{c^2}\chi_{uw}+\left(\frac{u^2}{c^2}-1\right)\chi_{ww}=0. \tag{30.23}$$

The same procedure used in (30.19) through (30.21), or a simple comparison of (30.17), (30.21), and (30.23), shows that the characteristic curves of (30.23) in the hodograph (u, w)-plane are defined by

$$\frac{w_\alpha}{u_\alpha}=\left(\frac{dw}{du}\right)_{\Gamma_\pm}=\frac{-\frac{uw}{c^2}\pm\sqrt{\frac{u^2+w^2}{c^2}-1}}{\frac{w^2}{c^2}-1}. \tag{30.24}$$

The characteristic curve Γ_- in the hodograph (u, w)-plane is orthogonal to the characteristic curve C_+ in the physical (x, z)-plane if we superimpose the two planes so that the velocity vectors coincide. This may be easily shown by rotating

the axes for (30.21) and (30.24) so that $w=0$ (see Fig. 40); then the equations for the slopes of the characteristic curves C_+ and Γ_- simplify to

$$\left(\frac{dz}{dx}\right)_{C_+} = \frac{1}{\sqrt{\frac{u^2}{c^2}-1}} = \frac{1}{\sqrt{F^2-1}} = -\frac{1}{\left(\frac{dw}{du}\right)_{\Gamma_-}}. \tag{30.25}$$

Similarly, Γ_+ is orthogonal to C_- when the planes are superimposed so that the velocity vectors are coincident (see Fig. 40).

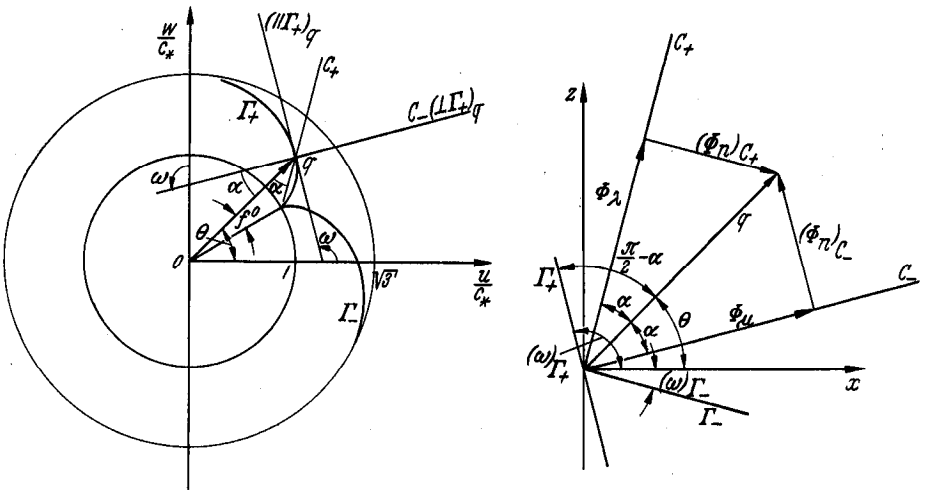

Fig. 40. Characteristic directions in the hodograph (u, w)-plane and the physical (x, z)-plane.

Eqs. (30.24) and (30.25) show that along any characteristic curve there exists a simple solution which is independent of the boundary conditions of a particular problem, for we can directly integrate (30.25) with axes rotated so that $w=0$ and hence $dw = u\,d\vartheta$:

$$\left(\frac{dw}{du}\right)_{\Gamma_-} = \left(\frac{u\,d\vartheta}{du}\right)_{\Gamma_-} = -\sqrt{\frac{u^2}{c^2}-1} = -\sqrt{F^2-1},$$

We integrate[1] (30.25) as follows:

$$\left.\begin{aligned} \int_{\Gamma_-} d\vartheta &= -\int_{\Gamma_-} \sqrt{\frac{u^2}{c^2}-1}\,\frac{du}{u} = -\int_{\Gamma_-} \frac{\sqrt{F^2-1}}{1+\frac{1}{2}F^2}\,\frac{dF}{F}, \\ |\Delta\vartheta| &\equiv \sqrt{3}\tan^{-1}\sqrt{\tfrac{1}{3}(F^2-1)} - \tan^{-1}\sqrt{F^2-1} = f(F). \end{aligned}\right\} \tag{30.26}$$

Consequently (30.26) provides a general solution, independent of the boundary conditions in the physical plane, for any two-dimensional potential flow that possesses the property of having simple waves in the given region, so that the end of the velocity vector follows Γ_- in the hodograph plane. The numerical values from (30.26) are indicated in Fig. 40 and are tabulated in Table 1 on page 688 [taken from PREISWERK (1938)].

The useful relation between c and (u, w) that was used to integrate (30.26) and calculate Table 1 is obtained by multiplying the first equation in (30.15)

[1] See (30.27) and (30.29) which show that with $w=0$

$$\frac{du}{u} = -\frac{d(c^2)}{u^2} = +\frac{c_0^2}{u^2}\left(1+\frac{1}{2}F^2\right)^{-2} F\,dF = +\frac{dF}{F(1+\frac{1}{2}F^2)}.$$

by dx and the second equation by dz, and then adding them. One obtains successively

$$\left.\begin{aligned} &u(u_x\,dx + u_z\,dz) + w(w_x\,dx + w_z\,dz) = -[(c^2)_x\,dx + (c^2)_z\,dz],\\ &u\,du + w\,dw = -d(c^2) = -g\,d\eta,\\ &\tfrac{1}{2}(u^2+w^2) + c^2 = \text{const} = \tfrac{1}{2}(u^2+w^2) + g(h_0+\eta). \end{aligned}\right\} \tag{30.27}$$

Therefore

$$\left.\begin{aligned} \tfrac{1}{2}(u^2+w^2) + c^2 &= \tfrac{1}{2}(u^2+w^2) + g(h_0+\eta)\\ &= g\,h_0 = \tfrac{1}{2}(u^2+w^2)_{\max} = \tfrac{3}{2}c_*^2 = \tfrac{1}{2}q^2 + c^2 = \tfrac{1}{2}q_{\max}^2, \end{aligned}\right\} \tag{30.28}$$

where (see Fig. 41) h_0 is the still water depth (or stagnation total head depth) that corresponds to $u_0^2 + w_0^2 = 0 = \eta_0$, $(u^2+w^2)_{\max}$ is the limiting resultant velocity

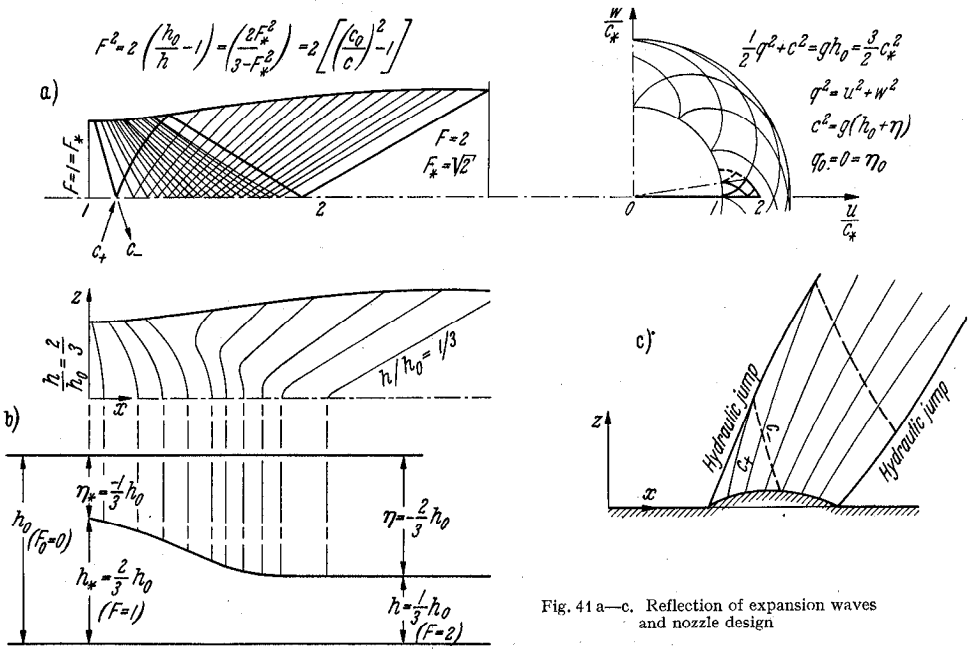

Fig. 41 a—c. Reflection of expansion waves and nozzle design

squared which is approached when the depth of flowing water approaches zero ($\eta \to -h_0$), and c^* is the speed when the resultant velocity $\sqrt{u^2+w^2} = c^*$ is critical ($F=1$), so that

$$\left.\begin{aligned} &c_* = \sqrt{g(h_0+\eta^*)} = \sqrt{\frac{2}{3}g\,h_0} = \sqrt{\frac{2}{3}\left[\frac{1}{2}c_*^2 + g(h_0+\eta_*)\right]} = \sqrt{\frac{1}{3}(u^2+w^2)_{\max}},\\ &\left(\frac{c_*}{c_0}\right)^2 = \frac{c_*^2}{g\,h_0} = \frac{2}{3} = -2\frac{\eta_*}{h_0},\\ &\frac{\eta_*}{h_0} = -\frac{1}{3}, \qquad \frac{h_0+\eta_*}{h_0} = \frac{2}{3}, \qquad \frac{(u^2+w^2)_{\max}}{c_*^2} = 3,\\ &\left(\frac{c_0}{c}\right)^2 = \frac{g\,h_0}{c^2} = 1 + \frac{u^2+w^2}{2c^2} = 1 + \frac{1}{2}F^2 = \left(\frac{c_0}{c_*}\right)^2\left(\frac{c_*}{c}\right)^2 = \frac{3}{2}\left(\frac{c_*}{c}\right)^2 = \frac{h_0}{h},\\ &F^2 = \frac{u^2+w^2}{c^2} = \left(\frac{c_*}{c}\right)^2 F_*^2 = \frac{2F_*^2}{3-F_*^2},\\ &F_*^2 = \frac{u^2+w^2}{c_*^2} = \left(\frac{c}{c_*}\right)^2 F^2 = \frac{3F^2}{2+F^2}. \end{aligned}\right\} \tag{30.29}$$

It is very useful to note that Eqs. (30.26) through (30.29) may all be obtained directly from the two-dimensional isentropic gas-flow equations by simply letting the specific heat ratio $\gamma = 2$ and $F \equiv M$, $F_* \equiv M_*$, as had been previously shown by PREISWERK (1938) [see also COURANT and FRIEDRICHS (1948)].

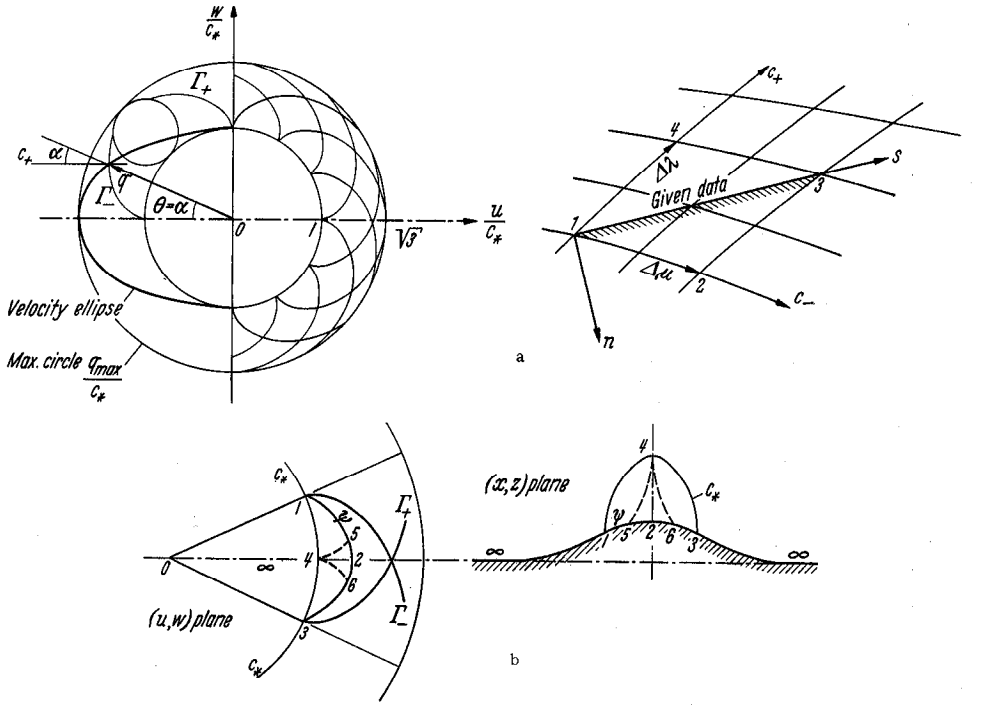

Fig. 42 a and b. Hodograph (u, w)-plane characteristic epicycloids.

The Riemann invariants for the characteristic curves (C_+, C_-) will now be determined. First we can show that the velocity component normal to the characteristic curves is always the local velocity of the shallow-water wave propagation, $c(x, z)$. We do this by writing (30.21) as

$$\left.\begin{aligned} (u\,dz - w\,dx)^2_{C_+} &= c^2\,[(dx)^2 + (dz)^2]_{C_+} = c^2\,(d\lambda)^2_{C_+}, \\ c^2 &= \left(u\,\frac{dz}{d\lambda} - w\,\frac{dx}{d\lambda}\right)^2_{C_+} = (\varphi_x x_n + \varphi_z z_n)^2_{C_+} = (\varphi_n)^2_{C_+}, \end{aligned}\right\} \tag{30.30}$$

since the relation between the normal direction (n), and the tangential direction (λ) along the characteristic curve (C_+) is given by (see Fig. 40)

$$\left(\frac{dx}{dn}\right)_{C_+} = \left(\frac{dz}{d\lambda}\right)_{C_+}, \left(\frac{dz}{dn}\right)_{C_+} = -\left(\frac{dx}{d\lambda}\right)_{C_+}.$$

Similarly, if μ is the tangential direction along C_-,

$$c^2 = \left(u\,\frac{dz}{d\mu} - w\,\frac{dx}{d\mu}\right)^2_{C_-} = (\varphi_x x_n + \varphi_z z_n)^2_{C_-} = (\varphi_n)^2_{C_-}.$$

Also, from Fig. 40 and (30.21)

$$\tan\alpha = \left(\frac{dz}{dx}\right)_{C_\pm,\,\vartheta=0} = \pm\frac{1}{\sqrt{F^2-1}}, \qquad \sin\alpha = \frac{\pm 1}{F} = \pm\frac{c}{q} \tag{30.31}$$

where q is the resultant velocity magnitude. Hence

$$\left.\begin{aligned} &q^2 = (u^2 + w^2) = (\varphi_\lambda^2 + c^2) = (\varphi_\mu^2 + c^2), \qquad \vartheta = \tan^{-1}\frac{w}{u}, \\ &u = q\cos\vartheta, \qquad w = q\sin\vartheta, \\ &\varphi_n = c = q\sin\alpha, \qquad \varphi_\lambda = q\cos\alpha = \varphi_\mu. \end{aligned}\right\} \tag{30.32}$$

Substituting (30.31) and (30.32) into (30.21) and (30.24) we obtain

$$\left(\frac{dz}{dx}\right)_{C_\pm} = \frac{\dfrac{\cos\vartheta\sin\vartheta}{\sin^2\alpha} \pm \dfrac{1}{\tan\alpha}}{\dfrac{\cos^2\vartheta}{\sin^2\alpha} - 1} = \tan(\vartheta \pm \alpha), \tag{30.33}$$

$$\left(\frac{dw}{du}\right)_{\Gamma_\mp} = \frac{-\dfrac{\cos\vartheta\sin\vartheta}{\sin^2\alpha} \pm \dfrac{1}{\tan\alpha}}{\dfrac{\sin^2\vartheta}{\sin^2\alpha} - 1} = -\cot(\vartheta \pm \alpha). \tag{30.34}$$

Therefore, as proven before in (30.25),

$$\left(\frac{dz}{dx}\right)_{C_+}\left(\frac{dw}{du}\right)_{\Gamma_-} = -1 = \left(\frac{dz}{dx}\right)_{C_-}\left(\frac{dw}{du}\right)_{\Gamma_+}, \tag{30.35}$$

that is, as shown in Fig. 40, the C_+ characteristic curves in the physical (x, z) plane are at every corresponding point orthogonal to the Γ_- characteristic curves in the hodograph (u, w) plane. All these results are the same as in the gas-dynamics case where the $C_\pm$ characteristic curves are referred to as the Mach lines since, as shown by (30.30), the normal velocity component is always the local speed of sound.

Now, as shown in Fig. 40,

$$\left(\frac{dw}{du}\right)_{\Gamma_-} = \tan\omega_{\Gamma_-}; \qquad \omega_{\Gamma_-} = \vartheta + \alpha - \frac{1}{2}\pi,$$

$$\left(\frac{dw}{du}\right)_{\Gamma_+} = \tan\omega_{\Gamma_+}; \qquad \omega_{\Gamma_+} = \vartheta - \alpha + \frac{1}{2}\pi;$$

therefore (30.33) may be written as

$$\left(\frac{dz}{dx}\right)_{C_+} = \tan(\vartheta + \alpha) = \tan\left(\omega_{\Gamma_-} + \frac{1}{2}\pi\right),$$

$$\left(\frac{dz}{dx}\right)_{C_-} = \tan(\vartheta - \alpha) = \tan\left(\omega_{\Gamma_+} - \frac{1}{2}\pi\right).$$

Consequently the Riemann invariants are given by

$$R = \vartheta + \alpha - \omega_{\Gamma_-} - \tfrac{1}{2}\pi, \qquad S = \vartheta - \alpha - \omega_{\Gamma_+} + \tfrac{1}{2}\pi.$$

These may be simplified by calculating

$$\omega_{\Gamma_-} = \arctan\left(\frac{dw}{du}\right)_{\Gamma_-} = -\sqrt{3}\,\operatorname{arccot}\left[\sqrt{\frac{3}{F^2-1}}\right] = -\sqrt{3}\arctan\left[\sqrt{\frac{F^2-1}{3}}\right]$$

from (30.24) and Fig. 40 since

$$\frac{1}{\sqrt{F^2-1}} = |\tan\alpha| = \sqrt{\frac{1}{3}}\left|\cot\left(\frac{\omega}{\sqrt{3}}\right)\right|$$

[or see COURANT and FRIEDRICHS (1948, p. 266)].

Table 1.

f (deg.)	$1+\frac{\eta}{h_0}$	F_*	F	K	f (deg.)	$1+\frac{\eta}{h_0}$	F_*	F	K
0	2/3	1.000	1.000	∞	26	0.234	1.516	2.56	−0.160
1	0.624	1.062	1.098	2.68	27	0.223	1.527	2.64	−0.177
2	0.598	1.101	1.160	2.07	28	0.212	1.538	2.73	−0.196
3	0.576	1.129	1.214	1.40	29	0.201	1.549	2.82	−0.216
4	0.555	1.156	1.267	1.014	30	0.190	1.559	2.92	−0.234
5	0.535	1.182	1.319	0.758	31	0.180	1.569	3.02	−0.252
6	0.516	1.207	1.371	0.590	32	0.170	1.579	3.13	−0.271
7	0.498	1.229	1.422	0.476	33	0.160	1.588	3.24	−0.291
8	0.481	1.249	1.470	0.394	34	0.151	1.597	3.36	−0.313
9	0.464	1.269	1.520	0.318	35	0.141	1.605	3.49	−0.336
10	0.448	1.288	1.570	0.263	36	0.132	1.613	3.63	−0.36
11	0.432	1.306	1.622	0.215	37	0.123	1.621	3.78	−0.38
12	0.417	1.323	1.674	0.170	38	0.115	1.629	3.93	−0.40
13	0.402	1.340	1.727	0.133	39	0.107	1.637	4.01	−0.43
14	0.387	1.356	1.781	0.103	40	0.099	1.644	4.26	−0.46
15	0.373	1.372	1.835	0.072	41	0.092	1.651	4.44	−0.49
16	0.359	1.387	1.89	0.046	42	0.085	1.657	4.63	−0.52
17	0.345	1.402	1.95	0.020	43	0.078	1.663	4.85	−0.54
18	0.331	1.416	2.01	−0.004	44	0.072	1.669	5.08	−0.58
19	0.318	1.430	2.07	−0.028	45	0.066	1.675	5.33	−0.62
20	0.305	1.444	2.13	−0.050	46	0.060	1.681	5.62	−0.66
21	0.292	1.457	2.20	−0.071	47	0.054	1.686	5.95	−0.70
22	0.280	1.470	2.27	−0.089	48	0.048	1.691	6.30	−0.75
23	0.268	1.482	2.34	−0.108	49	0.043	1.696	6.68	−0.81
24	0.256	1.494	2.41	−0.126	50	0.038	1.700	7.11	−0.86
25	0.245	1.505	2.48	−0.143	65°53′	0	$\sqrt{3}$	∞	$-\infty$

Therefore

$$R = \vartheta + \arctan\frac{1}{\sqrt{F^2-1}} - \frac{\pi}{2} + \sqrt{3}\arctan\sqrt{\frac{F^2-1}{3}}$$

$$= \vartheta + \sqrt{3}\arctan\sqrt{\frac{F^2-1}{3}} - \arctan\sqrt{F^2-1} = \vartheta + f(F),$$

$$S = \vartheta - \arctan\frac{1}{\sqrt{F^2-1}} + \frac{\pi}{2} - \sqrt{3}\arctan\sqrt{\frac{F^2-1}{3}}$$

$$= \vartheta - \sqrt{3}\arctan\sqrt{\frac{F^2-1}{3}} + \arctan\sqrt{F^2-1} = \vartheta - f(F),$$

where $f(F)$ is given by (30.26) and Table 1. Consequently the Riemann invariants are very simply expressed for the characteristic curves in the physical plane as

$$\vartheta - f(F) = \text{const on } C_+, \quad \vartheta + f(F) = \text{const on } C_-. \tag{30.36}$$

The function $f(F)$, which was derived from the fact that the end point of the velocity vector follows a characteristic in the hodograph plane in (30.26), is seen to have important physical significance, and directly provides the Riemann invariants for the steady two-dimensional potential flow. In gas dynamics $f(F) \equiv f(M)$ is referred to as the Prandtl-Meyer expansion function and, in the form in which it is given in Table 1, it corresponds to the supersonic free expansion about a sharp corner as shown in Fig. 43 for the centered simple wave with a specific heat ratio $\gamma = 2$. Since this Prandtl-Meyer function is so important, let us re-derive it on another basis that will further illustrate its physical significance. From the fact that f forms the Riemann invariant it is evident that u and w cannot be independent of one another on any such simple characteristic.

Consequently, if we write the original potential equation (30.18) in the physical plane as

$$\left(\frac{u^2}{c^2}-1\right)u_x+2\frac{u\,w}{c^2}u_y+\left(\frac{w^2}{c^2}-1\right)w_y=0$$

and introduce $w=w(u)$ so that

$$w_y=u_y\,w'(u),\quad u_x\,w'(u)=w_x=\varphi_{xz}=u_y,$$

we obtain

$$\left(\frac{u^2}{c^2}-1\right)\frac{u_y}{w'}+2\frac{u\,w}{c^2}u_y+\left(\frac{w^2}{c^2}-1\right)u_y\,w'=0$$

or

$$\frac{dw}{du}=w'(u)=\frac{\dfrac{-u\,w}{c^2}\pm\sqrt{\dfrac{u^2+w^2}{c^2}-1}}{\dfrac{w^2}{c^2}-1}. \tag{30.24'}$$

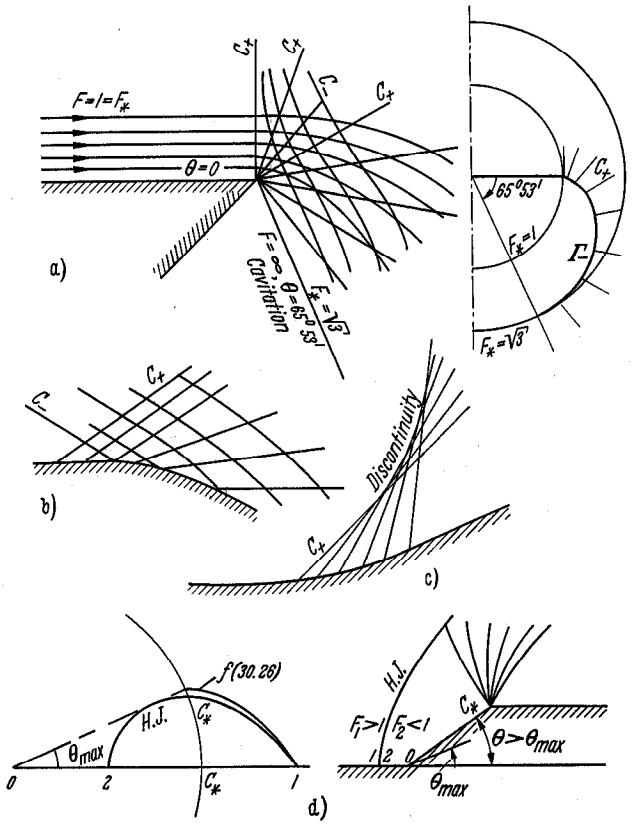

Fig. 43a–d. Simple waves and the formation of hydraulic jumps. (a) Complete centered simple expansion wave. (b) Simple(C_+) expansion waves. (c) Simple (C_+) compression waves forming a discontinuous (hydraulic jump) increase in water depth. (d) Detached hydraulic jump.

This derivation gives exactly the same result as in (30.24) and verifies the fact that discontinuities can occur in the first derivatives normal to a characteristic curve. If we introduce (30.32) into (30.24) we obtain the equivalent of (30.26)

$$\frac{1}{q}\frac{dq}{d\vartheta}=\tan\alpha=\frac{1}{\sqrt{F^2-1}} \tag{30.37}$$

which again has $f(F)$ as the general integral because (30.28) shows that

$$\frac{d\vartheta}{\sqrt{F^2-1}} = \frac{dq}{q} = \frac{d(q/c_*)}{(q/c_*)} = \frac{dF_*}{F_*} = \frac{1}{1+\frac{1}{2}F^2}\,\frac{dF}{F}. \tag{30.38}$$

However, neither of these methods gives the direct proof that $f(F)$ provides the Riemann invariant. This fact may be proved directly by the following derivation which utilizes the velocity component φ_λ along the C_+ characteristic, and $\varphi_n = c$, from (30.30), normal to C_+ as shown in Fig. 40. Hence

$$\left.\begin{aligned} \varphi_\lambda &= q\cos\alpha, \quad \varphi_n = c = q\sin\alpha, \\ d\varphi_\lambda &= \cos\alpha\, dq - q\sin\alpha\, d\alpha = c(d\vartheta - d\alpha), \\ \lambda_x &= 1/\sin(\vartheta+\alpha), \quad \mu_x = 1/\sin(\vartheta-\alpha) \end{aligned}\right\} \tag{30.39}$$

since, from (30.37),

$$dq = \frac{\sin\alpha}{\cos\alpha}\, q\, d\vartheta.$$

Then from (30.28) and (30.32) we have

$$\left.\begin{aligned} \tfrac{1}{2}q^2 + c^2 &= \tfrac{1}{2}(\varphi_\lambda^2 + \varphi_n^2) + c^2 = \tfrac{1}{2}\varphi_\lambda^2 + \tfrac{3}{2}c^2 = \tfrac{1}{2}q_{\max}^2 = \tfrac{3}{2}c_*^2, \\ c^2 &= \tfrac{1}{3}(q_{\max}^2 - \varphi_\lambda^2) = c_*^2 - \tfrac{1}{3}\varphi_\lambda^2, \end{aligned}\right\} \tag{30.40}$$

so that (30.39) may be written

$$\left.\begin{aligned} \vartheta - \alpha + \text{const} &= \int \frac{d(\varphi_\lambda)}{c} = \int \frac{d(\varphi_\lambda)}{\sqrt{\frac{1}{3}(q_{\max}^2 - \varphi_\lambda^2)}} = \sqrt{3}\int \frac{d(\varphi_\lambda/q_{\max})}{\sqrt{1-(\varphi_\lambda/q_{\max})^2}} \\ &= \sqrt{3}\arcsin\left(\frac{\varphi_\lambda}{q_{\max}}\right) = \sqrt{3}\arcsin\left(\frac{\varphi_\lambda}{\sqrt{3c^2+\varphi_\lambda^2}}\right) = \sqrt{3}\arctan\left(\frac{\varphi_\lambda}{c\sqrt{3}}\right) \end{aligned}\right\} \tag{30.41}$$

This may be finally written in terms of (F) alone by noting from (30.39) that

$$\frac{\varphi_\lambda}{c} = \frac{\varphi_\lambda}{\varphi_n} = \frac{q\cos\alpha}{q\sin\alpha} = \frac{1}{\tan\alpha} = \sqrt{F^2-1}.$$

Consequently (30.41) reduces to

$$\left.\begin{aligned} &\vartheta(F) - \sqrt{3}\arctan\left(\sqrt{\frac{1}{3}(F^2-1)}\right) - \arctan\frac{1}{\sqrt{F^2-1}} + \text{const} \\ &= \vartheta(F) - \sqrt{3}\arctan\left(\sqrt{\frac{1}{3}(F^2-1)}\right) + \arctan\sqrt{F^2-1} = \vartheta - f(F) = \text{const}, \end{aligned}\right\} \tag{30.42}$$

where $f(F)$ is the same Prandtl-Meyer function as given in (30.26) and Table 1. Therefore we have proven that the Riemann invariants are given by (30.36) and (30.26). In addition to the relation between f and F in (30.26) it is sometimes convenient to use one of the following:

$$\left.\begin{aligned} f(\alpha) &= \sqrt{3}\,\text{arc cot}\,(\sqrt{3}\tan\alpha) + \alpha - \frac{1}{2}\pi \\ &= f(F_*) = \sqrt{3}\arctan\sqrt{\frac{F_*^2-1}{3-F_*^2}} - \arctan\sqrt{\frac{F_*^2-1}{1-\frac{1}{3}F_*^2}} = \frac{\lambda+\mu}{2} \end{aligned}\right\} \tag{30.26'}$$

It now follows that a numerical solution can be obtained for the general problem in which both families of characteristics represent curved non-simple waves by carrying on a simultaneous finite-difference solution in the physical (x, z)-plane with (30.33), and in the hodograph (u, w)-plane by (30.26), (30.34), and (30.36). Almost any initial- or boundary-value data can be handled in this

manner as long as the curve on which the data are given is not coincident with a characteristic curve. The solution cannot be obtained in the neighborhood of any portion of the boundary-value curve that happens to be tangent to any characteristic curve, because, as proven by (30.20), the solution is indeterminate for boundary-value data given on a characteristic. It is easily seen by this finite-difference method that the data along a smooth non-characteristic curve can only determine the solution inside the quadrilateral formed by the characteristic curves passing through its end points (Fig. 42) [see, e.g., PREISWERK (1938) or COURANT and FRIEDRICHS (1948)]. This well-known behavior of hyperbolic-type partial differential equations is most directly demonstrated by writing them in their normal or canonical form by transforming the coordinates to curvilinear axes which are the characteristic curves themselves. For example, PREISWERK (1938) transforms the equivalent of (30.23) onto the curvilinear characteristic-coordinate (λ, μ) system to obtain

$$\left.\begin{aligned} f(F_*) &= \tfrac{1}{2}(\lambda+\mu), \quad \vartheta = \tfrac{1}{2}(\lambda-\mu), \\ \chi_{\lambda\mu} &= -K(\lambda,\mu)\,(\chi_\lambda+\chi_\mu), \\ K(\lambda,\mu) &= \frac{F_*^2(1-\frac{1}{2}F_*^2)}{\sqrt{3}\,(3-F_*^2)^{\frac{1}{2}}\,(F_*^2-1)^{\frac{5}{2}}}. \end{aligned}\right\} \tag{30.43}$$

This normal or canonical form is so useful in carrying out the finite-difference method of solution that the values of K have also been included in Table 1. It can be used in the following type of approximation, as indicated in Fig. 42 where (1, 3) are known values and (2, 4) are to be calculated,

$$\left.\begin{aligned} \chi_\lambda &= \frac{\chi_4-\chi_1}{\lambda_4-\lambda_1}, \quad \chi_\mu = \frac{\chi_2-\chi_1}{\mu_2-\mu_1}, \\ \left(-\frac{K_1+K_3}{2}\right)(\chi_\lambda+\chi_\mu) &= \chi_{\lambda\mu} = \frac{(\chi_3+\chi_1)-(\chi_4+\chi_2)}{(\lambda_4-\lambda_1)\,(\mu_2-\mu_1)}. \end{aligned}\right\} \tag{30.43'}$$

Consequently, if the data were given on only one characteristic curve the method would fail since the values must be known on *both* characteristics, or on the non-characteristic curve s in Fig. 42, so that one can also write

$$\chi_s = \chi_\lambda \lambda_s + \chi_\mu \mu_s = g(s),$$
$$\chi_n = \chi_\lambda \lambda_n + \chi_\mu \mu_n = G(s).$$

The numerical method of solution by finite differences following (30.43') is known as the "lattice-point method" and replaces the original partial differential equation (30.43) by a set of linear algebraic equations. The other commonly used semi-graphical method of solving hyperbolic partial differential equations is called the network or "mesh method" and can be illustrated by writing (30.43) in the form

$$\left.\begin{aligned} \Delta\chi_\lambda &= -K(\chi_\lambda+\chi_\mu)\,\Delta\mu, \\ \Delta\chi_\mu &= -K(\chi_\lambda+\chi_\mu)\,\Delta\lambda. \end{aligned}\right\} \tag{30.43''}$$

The average value at the center of each mesh formed by the characteristic network is used for the trial and error numerical calculation of each Δ increment. The increments are drawn tangent to the characteristic curves as indicated in Fig. 42. The simultaneous semi-graphical solution must be carried out in the physical plane as shown in Fig. 42 by using (30.33) and writing (30.39) and (30.41) in finite difference form.

As a further aid to numerical and graphical solutions it is useful to plot $f(F_*)$ from (30.26′) or Table 1 on the hodograph $(u/c_*, w/c_*)$-plane as shown in Fig. 42. The single curve defined by Table 1 may be drawn and then rotated by equal increments of $\Delta\vartheta$, or the construction may be accomplished entirely by graphical means as indicated in Fig. 42 by rotating the small circle upon the inner unit circle representing critical flow, while the outer maximum circle has a radius of $\sqrt{3}$ representing $q_{\max}/c_*$ from (30.29). This geometrical construction yields $f(F_*)$ since it is an epicycloid, as proven by PREISWERK (1938), or COURANT and FRIEDRICHS (1948, p. 262). All simple waves must follow the characteristic epicycloid in the hodograph plane because simple waves are defined by (30.37) which has been proven to have $f(F_*)$ as its integral. It can be shown that all streamlines corresponding to non-simple waves must lie within the corresponding characteristic epicycloids as indicated in Fig. 42, since the streamline must have

$$\left|\frac{1}{F_*}\left(\frac{dF_*}{d\vartheta}\right)_{\psi\,\text{const}}\right| \leqq \tan\alpha \tag{30.44}$$

unless a finite discontinuity corresponding to a hydraulic jump (or shock wave in a gas) is formed.

Another useful aid in the hodograph graphical construction is the velocity ellipse, which is also drawn in Fig. 42. Wherever the velocity vector q touches the curve of the ellipse, it will be found that the major axis of the ellipse is in the direction of the tangent to the corresponding characteristic (either C_+ or C_-) in the physical plane because, as a consequence of (30.29) and (30.32), if we assume that $\vartheta = \alpha$ then

$$(w/c_*)^2 = F_*^2 \sin^2\alpha = F_*^2/F^2 = \tfrac{1}{2}(3 - F_*^2),$$

$$(u/c_*)^2 = F_*^2(1 - \sin^2\alpha) = \tfrac{3}{2}(F_*^2 - 1),$$

$$\tfrac{2}{3}(u/c_*)^2 + 1 = F_*^2 = 3 - 2(w/c_*)^2,$$

or

$$\tfrac{1}{3}(u/c_*)^2 + (w/c_*)^2 = 1 = [\tfrac{1}{3}(\varphi_\mu/c_*)^2 + (c/c_*)^2]_{C_-,\,\vartheta=0} = [\tfrac{1}{3}(\varphi_\lambda/c_*)^2 + (c/c^*)^2]_{C_+,\,\vartheta=0}. \tag{30.45}$$

This gives the velocity ellipse shown in Fig. 42 with a major axis of $\sqrt{3}$ and a minor axis of unity. The major axis is always at the Mach angle α with respect to the velocity vector q because we find from (30.28) and (30.32) that when $\alpha = \vartheta$

$$(w/c_*)^2 = (\varphi_n/c_*)^2 = (c/c_*)^2 = 1 - \tfrac{1}{3}(u/c_*)^2.$$

As in the previous case of unsteady one-dimensional flow over a flat bottom we can obtain very simple solutions for the case of simple waves. In this case there is an analogy between the (t, x) diagram and the (x, z) diagram [see, e.g., COURANT and FRIEDRICHS (1948)]. As before, the simple wave corresponds to having the characteristics in the (x, z)-plane of one family become straight lines, as in the examples shown in Fig. 43, so that $(q, \vartheta, \alpha, \eta)$ are all constant on the straight line $dz/dx = \text{const}$ in the physical plane. Therefore any given straight characteristic line has all of its properties determined by $f(F_*)$ from (30.26) and each of the straight lines in the physical plane maps onto a single point of the same single characteristic epicycloid in the hodograph plane. The characteristics of the other family remain curved in the physical plane and map in a unique continuous manner upon the corresponding characteristic epicycloid arcs in the hodograph plane. As before, in a simple wave these curved characteristics are not required for a numerical solution.

Common examples of simple-wave problems are shown in Fig. 43, and they always occur whenever a region of constant uniform properties adjoins a region having any variation in its properties, the two regions always being joined by a straight-line physical characteristic ($dz/dx = \text{const}$) as long as no finite discontinuities, corresponding to hydraulic jumps or shock waves, have been formed. These finite discontinuities correspond to an envelope of the straight characteristic lines that must form whenever the boundary-surface curves towards the oncoming flow, resulting in a flow compression or decrease of velocity and increase in water depth as indicated in Fig. 43. The solution is no longer single valued at, or downstream of the envelope so this region must be replaced by a hydraulic jump having a finite discontinuity.

If the local flow velocity and water depth are required only on the curved boundary itself, then neither family of characteristics has to be determined (except as a precaution to verify that no finite discontinuities have formed near the boundary due to flow compression). The solution on the curved boundary itself is given directly from Table 1 by simply measuring $f(F_*)$ as the value corresponding to (see Fig. 43)

$$f[F_*(\vartheta)] = f[F_{*\infty}] \pm \vartheta. \tag{30.46}$$

If this expression becomes zero it signifies that the supercritical flow has been compressed to critical speed and a detached hydraulic jump can occur as in Fig. 43.

Whenever disturbance waves enter along both families, either due to another boundary or by reflection from a hydraulic jump, as in Fig. 41, then the mixed region contains non-simple waves, and only a numerical solution, similar to the ones discussed in conjunction with (30.43), can yield the exact solution. However, an approximate solution for the particular cases shown in Fig. 41 can be obtained by approximating the curved characteristics in the non-simple region by means of simple-wave straight characteristic lines. The geometrical construction assumes that the curved boundary wall of the nozzle can be replaced by a series of straight chord lines which each have the same magnitude of $\Delta\vartheta$ at every corner, as depicted in Fig. 44. At each expansion corner it is assumed that the centered simple wave (corresponding to a portion of the complete Prandtl-Meyer expansion, f) can be approximated by a single physical characteristic that is the average of the actual expansion fan of characteristics. This is the (dz/dx) straight line that is normal to the midpoint of the $\Delta\vartheta$ epicycloid arc representing the expansion-angle change at this corner, as shown in Fig. 44. Similarly, the compression corner that turns into the flow is represented by the single compression simple wave that is normal to the midpoint of the $\Delta\vartheta$ epicycloid arc representing the compression angle change at this corner. It will be shown that the angle of this single average compression wave is actually the correct limiting value for a weak hydraulic jump. The geometrical construction is carried out in the manner indicated in Fig. 44. Whenever a streamline crosses one of these finite amplitude construction characteristics the flow is assumed to bend through the $\Delta\vartheta$ associated with the finite corner bend which supposedly produced this single finite wave. The corresponding construction in the hodograph plane transfers to the epicycloid arc that is normal to the single finite wave in the physical plane as shown in Fig. 44.

Also shown in Fig. 44 are the geometric constructions required for the reflection of these simple finite waves in the physical plane from either solid boundaries, or from free boundaries with constant water depth. In the reflection from a solid boundary the original boundary slope is again attained by the velocity

vector after passing through the reflected wave which has the same strength for flow deflection as the original oncoming finite simple wave. In the hodograph plane the streamline has gone from one family of epicycloids to the other, ending at the same value of ϑ. The completed solution for the flow inside a channel

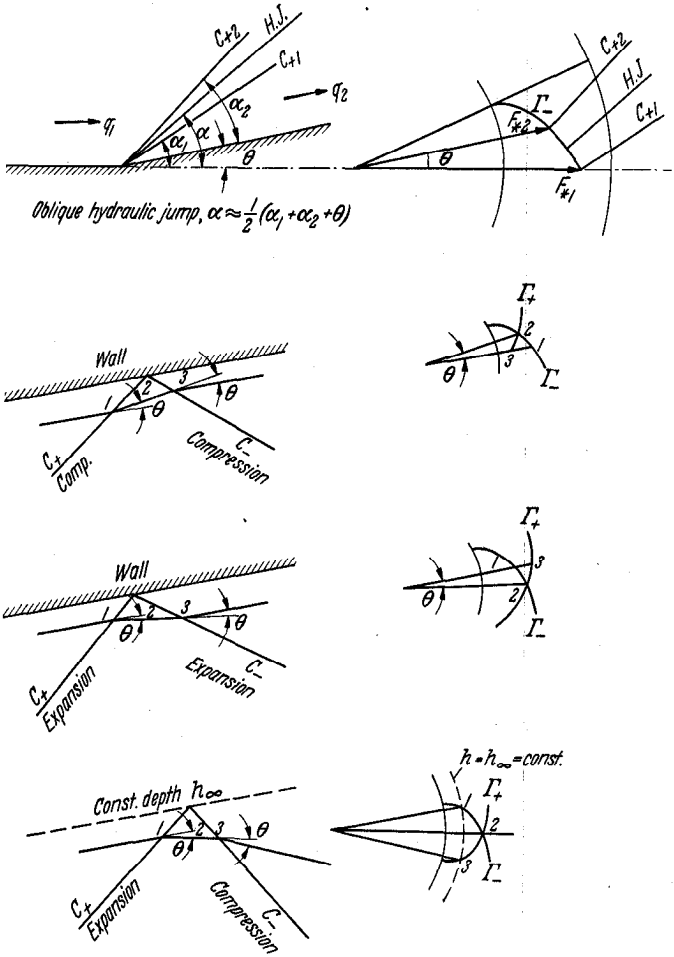

Fig. 44. Reflection of compression and expansion waves.

of varying width having supercritical flow ($F>1$) is presented in Fig. 41. For additional details and aids on the graphical constructions see PREISWERK (1938). As another example in Fig. 44, consider the reflection from a free jet, hydraulic jump, or any constant-water-depth free boundary, which must occur in such a manner that the same water depth is maintained after passing through the reflected wave which is not only on the opposite family of epicycloid arcs, but now must have the negative algebraic strength of the flow deflection of the original oncoming wave; consequently, the value of $\Delta\vartheta$ is exactly doubled after passing through the reflected wave. That is to say, unlike the ordinary reflection from a solid boundary, the reflection from a constant-depth free boundary results in the opposite type of wave, an expansion wave becoming a compression wave and vice versa.

In conclusion it must be noted that this two-dimensional steady-flow analysis is only valid for a flat horizontal bottom, as was already shown by (29.3) for the linearized equations. If the bottom slope varies, then the Riemann invariants do not exist, simple waves do not occur, and the numerical solution is much more complicated. However, there is an even more important criterion that must be satisfied before *any* of the solutions given so far can be applicable. This is the necessary requirement that all the perturbation quantities involved $(u-U,\ w,\ \eta)$ must be sufficiently small so that it is not necessary to introduce the second-order terms from Sect. 31. A satisfactory evaluation of this criterion, at least for F not too near unity, can be obtained by comparing the solutions of the non-linear equation (30.17) with the linearized equation (29.23) or (29.32). As is well-known in gas dynamics, and is apparent by inspection, (29.23) and (29.32) are not satisfactory for F approaching unity since additional terms must then be retained. For example, on the boundary profile itself, (29.3) for a flat horizontal bottom must include the additional term $3F^2(\varphi_x/U)\varphi_{xx}$, which corresponds to the "transonic approximation" of the gas dynamic equation (with a specific heat ratio $\gamma=2$) in the limit as F approaches unity. However, for the solution of the steady flow everywhere about a two-dimensional profile it may be necessary to use

$$(1-F^2)\,\varphi_{xx}+\varphi_{zz}=F^2\left[3\,\frac{\varphi_x}{U}\,\varphi_{xx}+2\,\frac{\varphi_z}{U}\,\varphi_{xz}\right] \tag{30.47}$$

since (29.29) indicates that far from the profile $w/U=\varphi_z/U\sim 1/z$, whereas $(u-U)/U=\varphi_x/U\sim 1/z^2$. In any case any radical increase in the order of magnitude of any perturbation term immediately indicates that the second-order terms discussed in Sect. 31 must be introduced, since the non-linear equation (28.1) and all the preceding results are based only on the first-order terms of the shallow-water theory.

γ) One-dimensional, steady, open-channel hydraulics and the hydraulic jump. see errata The reltations given in Eqs. (30.27) (30.28) and (39.29), and shown in Fig. 41, can be used in what is commonly known as the steady "one-dimensional" hydraulics of open-channel flow. Here we assume that even though the channel width $b(x)$ is varying, still the values of $q(x)$ and $\eta(x)$ do not depend upon z and therefore do not vary on any given cross-section. In conjunction with the steady "one-dimensional" concept it is necessary that $w\approx 0\approx\vartheta$. Consequently the basic equations to be used for a flat horizontal bottom are given by $q(x)=u(x)$ in (30.27), (30.28) and (30.29), and, in addition, by the "one-dimensional" continuity equation

$$b(x)\,h(x)\,u(x)=A(x)\,u(x)=Q=\left(\frac{\text{meters}^3}{\text{sec}}\right)=\text{const}, \tag{30.48}$$

where, from Fig. 41, $h(x)=h_0+\eta(x)=A(x)/b(x)$.

The validity of the "one-dimensional" assumption can be considerably in error if $b'(x)$ is large since it is obvious that in this case w or ϑ cannot be small. However, the "one-dimensional" approximation gives surprisingly good numerical values, even in supercritical flow *if* the channel is well designed as in Fig. 41 so as to maintain the flow as uniform as possible. However in supercritical flow the velocity over any cross-section remains uniform only near the design Froude number (F). PREISWERK (1938) gives the calculated and measured water depths in a Laval-type nozzle (the same one duplicated in Fig. 41) at various supercritical Froude numbers $(F>1)$. His results indicate that "one-dimensional" hydraulics gives a satisfactory approximation, having an error probably less than 10 %, even for critical or supercritical flow. This method should be especially

useful for subcritical flow since the more exact numerical solution is now very difficult to obtain because the simple method of characteristics is no longer applicable.

The most useful, and obviously the most accurate, application of "one-dimensional" hydraulics is to the constant-width rectangular-cross-section open-channel flow. In this application the friction effect of the vertical channel walls generally has a greater effect on the variation of $q(x, y, z)$ than would any of the more exact terms of the complete first-order shallow-water equations (28.1) which have been derived on the assumption of negligible viscosity effects. Consequently the

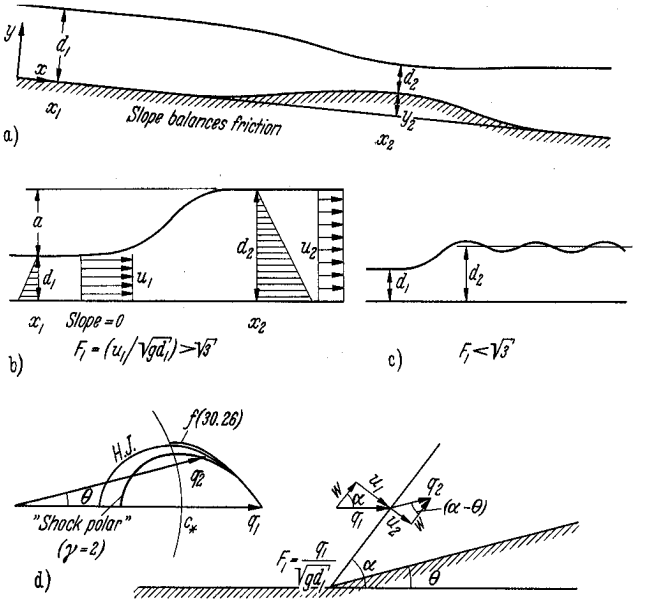

Fig. 45a—d. (a) One-dimensional flow over a sloping bottom, $|dy/dx| \ll 1$ so centrifugal force negligible. (b) Normal hydraulic jump. (c) Undulating hydraulic jump. (d) Oblique hydraulic jump with $w = w_1 = w_2$.

"one-dimensional" assumption that $q = u(x)$ provides a satisfactory approximation for the constant width (b), rectangular-cross-section, vertical-wall channel having $A(x) = b\,d(x)$. Even more important, this open-channel flow analysis may be further generalized, with but little additional difficulty, to apply to a bottom slope varying also with x. The "one-dimensional" continuity equation (30.48) then becomes

$$u(x)\,d(x) = \frac{Q}{b} = \text{const}, \tag{30.49}$$

where $d(x)$ is measured vertically from the varying bottom as shown in Fig. 45. The generalization of the Bernoulli equation (30.27) to include extraneous head losses (h_L), other than those due to friction, and local variations in the bottom contour $y(x)$, as shown in Fig. 45, may be written as

$$\left.\begin{aligned}(\text{specific energy}) &= \left(\frac{\text{kg meters}}{\text{kg}}\right) = (\text{meters}) = d(x) + \frac{u^2(x)}{2g} + y(x) + h_L(x) \\ &= d(x) + \frac{(Q/b)^2}{2g\,d^2(x)} + y(x) + h_L(x) = \text{const}.\end{aligned}\right\} \tag{30.50}$$

This assumes that in steady flow the work of gravity, through the known average slope of the flow, is wholly spent in overcoming the frictional resistance.

Another relation, that is necessary for calculating the sudden additional head loss h_L in hydraulic jumps or other discontinuous flow phenomenon, is given by the impulse-momentum relation [see KELVIN (1886), RAYLEIGH (1914), or BAKHMETEFF (1932)],

$$\left.\begin{aligned}(\text{specific momentum}) &= \left(\frac{\text{meters}^3}{\text{sec}^2}\right) = \frac{1}{2} g\, d^2(x) + d(x)\, u^2(x) \\ &= \frac{1}{2} g\, d^2(x) + \frac{(Q/b)^2}{d(x)}\end{aligned}\right\} \tag{30.51}$$

which is constant across the hydraulic jump over a flat horizontal bottom as shown in Fig. 45.

Eq. (30.50) with zero additional head loss ($h_L = 0$), gives the "one-dimensional" solution for the open-channel flow that has no finite discontinuities in the flow itself, and either has the hydraulic frictional resistance exactly balanced by the given average slope for steady flow (so that if $y = 0$ the surface slope is parallel to the bottom), or the hydraulic frictional resistance can be approximated by the Chézy formula for the case of varying open-channel flow [see BAKHMETEFF (1932) or STOKER (1957)]. A useful concept for nearly all solutions is the definition of the critical depth d_*, which corresponds to our previous definition of critical flow velocity in (30.28), that is, with $w \approx 0 \approx \vartheta$ we assume that

$$\left.\begin{aligned}u_* = c_* &= \sqrt{\frac{2}{3} g\, h_0} = \frac{u_{\max}}{\sqrt{3}}, \qquad F_* = 1 = F, \\ d_* &= \frac{2}{3} h_0 = \frac{c_*^2}{g} = \left[\frac{(Q/b)^2}{g}\right]^{\frac{1}{3}}.\end{aligned}\right\} \tag{30.52}$$

The last relation for d_* can be obtained either directly from (30.27), or by substituting the expression $u_* = \sqrt{\frac{2}{3} g h_0}$ into (30.50) with y and h_L both zero. Also from (30.29) we have

$$\left.\begin{aligned}\frac{d}{h_0} &= \frac{2}{2 + F^2}, \qquad F_*^2 = F^2 \left(\frac{c}{c_*}\right)^2 = \frac{3F^2}{2 + F^2}, \\ F^2 &= \frac{u^2}{g\, d} = \frac{(Q/b)^2}{g\, d^3} = \left(\frac{d_*}{d}\right)^3.\end{aligned}\right\} \tag{30.53}$$

As an example, if we apply Eqs. (30.50) and (30.52) to determine the flow relations between stations (1) and (2) in Fig. 45a we obtain, since h_L is generally negligible for a smooth variation in y_2,

$$\frac{d_2}{d_*} + \frac{1}{2}\left(\frac{d_*}{d_2}\right)^2 = \frac{d_1}{d_*} + \frac{1}{2}\left(\frac{d_*}{d_1}\right)^2 - \frac{y_2}{d_*}$$

as a satisfactory approximation for "one-dimensional" hydraulics, at least as long as y_2/d_* is sufficiently small. It is interesting to note that here is another resemblance to gas-dynamics behaviour since

$$\begin{aligned}\frac{y_2 + d_2}{d_*} < \frac{d_1}{d_*} > 1 \quad &\text{for } F_1 < 1, \\ \frac{y_2 + d_2}{d_*} > \frac{d_1}{d_*} < 1 \quad &\text{for } F_1 > 1.\end{aligned}$$

As another example, if we consider the hydraulic jump shown in Fig. 45b, now we find that a solution can only be obtained by using the impulse-momentum relation (30.51), thereby proving that the discontinuous change occurring in a hydraulic jump must result in a head loss. If the bottom slope is negligible, as

indicated in Fig. 45 b, then the impulse-momentum relation (30.51) may be written, with $Q/b = u_1 d_1 = u_2 d_2$, in the following manner, first given by RAYLEIGH (1914):

$$\left.\begin{aligned} &\frac{1}{2} g d_1^2 + d_1 u_1^2 = \frac{1}{2} g d_2^2 + \frac{(Q/b)^2}{d_2} = \frac{1}{2} g d_2^2 + \frac{(u_1 d_1)^2}{d_2}, \\ &F_1^2 = \frac{(Q/b)^2}{g d_1^3} = \frac{u_1^2}{g d_1} = \frac{1}{2} \frac{\left(\frac{d_2}{d_1}\right)^2 - 1}{1 - \frac{d_1}{d_2}} = \frac{1}{2} \frac{d_2}{d_1}\left(1 + \frac{d_2}{d_1}\right), \end{aligned}\right\} \tag{30.54}$$

or, if we let the actual rise in water level be $a = d_2 - d_1$,

$$F_1 = \frac{u_1}{\sqrt{g d_1}} = \left[1 + \frac{3}{2}\frac{a}{d_1} + \frac{1}{2}\left(\frac{a}{d_1}\right)^2\right]^{\frac{1}{2}}. \tag{30.55}$$

where

$$1 + \frac{a}{d_1} = \frac{d_2}{d_1} = \frac{1}{2}\left[\sqrt{1 + 8\frac{(Q/b)^2}{g d_1^3}} - 1\right] = \frac{1}{2}\left[\sqrt{1 + 8F_1^2} - 1\right]. \tag{30.56}$$

Similarly, (30.54) can also be solved for

$$F_2^2 = \frac{(Q/b)^2}{g d_2^3} = \frac{u_2^2}{g d_2} = \frac{1}{2}\frac{d_1}{d_2}\left(1 + \frac{d_1}{d_2}\right) = F_1^2\left(\frac{d_1}{d_2}\right)^3. \tag{30.57}$$

Eqs. (30.54) and (30.57) may be multiplied together to yield

$$u_1 u_2 = \frac{1}{2} g (d_1 + d_2) = c_{1*}^2 \left[\frac{3}{2 + F_1^2}\right]\left[\frac{1 + \sqrt{1 + 8F_1^2}}{4}\right] < c_{1*}^2 > c_{2*}^2. \tag{30.58}$$

The last inequality in (30.58) is obtained from (30.50) and (30.52) by noting that in any finite hydraulic jump the head loss must also be finite, so that $h_L = h_{0_1} - h_{0_2} > 0$ and (30.50) must be written as

$$\left.\begin{aligned} &d_1^2 + \frac{u_1^2}{2g} = d_2^2 + \frac{u_1^2}{2g}\left(\frac{d_1}{d_2}\right)^2 + h_{0_1} - h_{0_2}, \\ &h_L = h_{0_1} - h_{0_2} = \frac{1}{2} F_1^2 \frac{(1 - d_1/d_2)^3}{1 + d_2/d_1} d_2 \\ &\quad = \frac{1}{4} F_1^2 \left[\sqrt{1 + 8F_1^2} - 1\right] \frac{(1 - d_1/d_2)^3}{1 + d_2/d_1} d_1. \end{aligned}\right\} \tag{30.59}$$

Thus (30.52) and (30.59) give the total head ratio, and therefore the critical speed ratio, as

$$\left.\begin{aligned} \frac{h_{0_2}}{h_{0_1}} &= \left(\frac{c_{2*}}{c_{1*}}\right)^2 = 1 - \frac{h_L}{h_{0_1}} = \frac{d_{2*}}{d_{1*}} \\ &= \frac{(\sqrt{1 + 8F_1^2} - 1)^3 + 4F_1^2}{(\sqrt{1 + 8F_1^2} - 1)^2 (2 + F_1^2)} < 1. \end{aligned}\right\} \tag{30.60}$$

Consequently there is no direct analogy between finite hydraulic jumps and gas-dynamic shock waves, as was pointed out by PREISWERK (1938), since in gas dynamics the well-known Prandtl relation for normal shock waves gives $u_1 u_2 = c_*^2$, and c_* is constant through the shock wave [see, e.g., COURANT and FRIEDRICHS (1948, p. 146)]. The equations are similar only for the limiting case as the hydraulic jump vanishes so that $F_1 = F_2 = 1$, $d_2 = d_1$, and $h_{0_2} = h_{0_1}$. However this limiting process corresponds to the isentropic potential-flow case where there is an analogy for small perturbations over a flat horizontal bottom, as previously discussed. Also, as indicated by (30.59) the head loss and variation

in c_* could be neglected until the third-order terms become important, so that for F_1 near unity the first- and second-order terms of the hydraulic-jump relations correspond to the gas-dynamic shock-wave relations having a specific heat ratio $\gamma = 2$. However, this is identical to the known fact that weak shock waves may be considered isentropic to the third order of approximation; consequently the hydraulic analogy to compressible gas dynamics exists only for small perturbations in potential flow.

There is no direct analogy between the finite hydraulic jump and the gas-dynamic shock wave because the hydraulic jump has a head loss that must be included in the specific-energy equation (30.50). This head loss results in a loss of kinetic energy that is no longer available as flow energy since it is converted into an insignificant temperature rise in the water itself. In the gas dynamics energy equation the entropy increase through a shock wave of course corresponds to a loss of kinetic energy, but this is converted, through the increase of the temperature of the gas, into an adiabatic enthalpy increase that maintains constant flow energy through the shock wave [see, e.g., COURANT and FRIEDRICHS (1948, p. 125)]. The most unusual effect of this loss in flow energy (or h_L) in the hydraulic jump is revealed in (30.58) which shows that the flow velocity downstream of a hydraulic jump is always less than in the corresponding gas dynamics case, which maintains c_* constant so that $u_1 u_2 = c_*^2$. For example, in the gas-dynamic case when $F_1 \to \infty$, then $u_1/c_* \to \sqrt{3}$ (for $\gamma = 2$), and therefore $u_2/c_* \to 1/\sqrt{3}$. However, in a hydraulic jump (30.58) shows that $u_2/c_* \to 0$ when $F_1 \to \infty$ (or $u_1/c_* \to \sqrt{3}$).

The experimental investigations by BAKHMETEFF (1932) have shown that the hydraulic jumps in a horizontal rectangular channel are in excellent agreement with the predictions of the "one-dimensional" hydraulic equations (30.54) through (30.60). BAKHMETEFF found that depth increases as high as $10\,d_1$ were in excellent agreement with (30.56). However, he found that for Froude numbers of the oncoming flow less than $\sqrt{3}$ (i.e., $F_1 < \sqrt{3}$) the profile of the normal hydraulic jump developed undulations, and the relative length of transition became indeterminate because the undulating surface made the region of parallel flow increasingly remote from the start of the wave front, as indicated in Fig. 45 c. It is interesting to note that $F_1 = \sqrt{3}$ corresponds to the maximum absolute elevation that a hydraulic jump can reach with a given h_0 (although there is no limit to d_2/d_1), since (30.53) and (30.56) may be combined to give

$$\frac{d_2}{h_{0_1}} = \frac{1}{2 + F_1^2}\left(\sqrt{1 + 8F_1^2} - 1\right) \leqq \frac{4}{5}$$

which attains its maximum elevation of $\frac{4}{5} h_{0_1}$ above the channel bottom only for $F_1 = \sqrt{3}$; at this condition we have

$$\frac{d_2}{d_1} = 2, \quad F_2^2 = \frac{3}{8}, \quad \frac{h_L}{d_1} = \frac{1}{8}, \quad \frac{h_{0_2}}{h_{0_1}} = \frac{19}{20}, \quad u_1 u_2 = \frac{9}{10} c_{1_*}^2.$$

This shows that for all the undulating hydraulic jumps ($F_1 < \sqrt{3}$) the change in total head is less than 5 %; consequently these jumps can be approximated by the isentropic, potential-flow relations. This is of great aid in calculating the slant or oblique hydraulic jumps, as shown in Fig. 45 d, since the characteristic epicycloid values of $f(F_*)$, as given in Table 1, may be used in the manner indicated in (30.46) to approximate the change in F_*, F, or η upon turning through an angle ϑ by means of an oblique hydraulic jump whenever $d_2/d_1 \to 1$. The comparison between the value given by $f(F_1)$ in Table 1 for compression to $F_2 = 1$, is compared

with the exact values for the corresponding oblique hydraulic jumps in Fig. 46. It is seen that, although the gas-dynamic shock wave is not a satisfactory approximation for $F_1 > \sqrt{3}$, still the isentropic potential relation $f(F_1)$ provides an excellent approximation for much greater values of F_1 since the criterion for oblique hydraulic jumps is that the flow component normal to the discontinuity satisfy $F_1 \sin\alpha < \sqrt{3}$.

The exact relations for the oblique hydraulic jump are given by PREISWERK (1938) and can be obtained by simply adding the same velocity component ($w = w_1 = w_2$) tangent to both faces of the hydraulic jump as shown in Fig. 45 d.

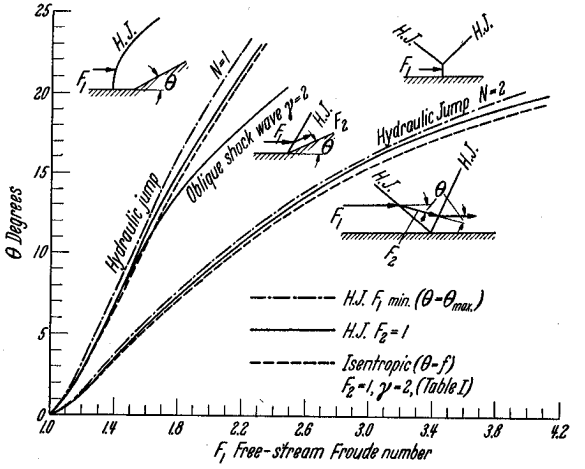

Fig. 46. Maximum flow deflection ($n = 1$), and reflection ($n = 2$).

This results in the following equations (which reduce to the preceding ones for a normal hydraulic jump by simply letting $\vartheta \to 0$ and $\alpha \to \pi/2$):

$$\left.\begin{aligned}
F_1^2 &= \frac{1}{2\sin^2\alpha}\,\frac{\tan\alpha}{\tan(\alpha-\vartheta)}\left[1+\frac{\tan\alpha}{\tan(\alpha-\vartheta)}\right] = \left[\frac{u_1/\sqrt{g\,d_1}}{\sin\alpha}\right]^2,\\
F_2^2 &= F_1^2\left(\frac{d_1}{d_2}\right)^3\left[\frac{\sin\alpha}{\sin(\alpha-\vartheta)}\right]^2 = \left[\frac{u_2/\sqrt{g\,d_2}}{\sin(\alpha-\vartheta)}\right]^2,\\
\frac{d_2}{d_1} &= \frac{\tan\alpha}{\tan(\alpha-\vartheta)} = \frac{1}{2}\left[\sqrt{1+8F_1^2\sin^2\alpha}-1\right] = \frac{u_1}{u_2},\\
\tan\vartheta &= \frac{\tan\alpha\left[\sqrt{1+8F_1^2\sin^2\alpha}-3\right]}{2\tan^2\alpha-1+\sqrt{1+8F_1^2\sin^2\alpha}},\\
\sin\alpha &= \frac{1}{F_1}\sqrt{\frac{1}{2}\left(\frac{d_2}{d_1}\right)\left(1+\frac{d_2}{d_1}\right)} = \frac{u_1/\sqrt{g\,d_1}}{F_1},\\
\sin(\alpha-\vartheta) &= \frac{1}{F_2}\sqrt{\frac{1}{2}\left(\frac{d_1}{d_2}\right)\left(1+\frac{d_1}{d_2}\right)} = \frac{u_2/\sqrt{g\,d_2}}{F_2}.
\end{aligned}\right\} \qquad (30.61)$$

The last two equations in (30.61) clearly show how the oblique hydraulic jump approaches the same value as given by the isentropic, potential relation $f(F_1)$ at *any* value of F_1 as long as $d_2/d_1 \to 1$, since they reduce to the isentropic, potential characteristic curve given by (30.31) whenever $\vartheta \to 0$ and $d_2/d_1 \to 1$. As a matter of fact, as previously mentioned, (30.61) shows that the oblique hydraulic jump angle (α) can be approximated as in Fig. 44 by

$$\alpha = \frac{1}{2}\left(\arcsin F_1^{-1} + \arcsin F_2^{-1} + \vartheta\right) + O\left(\frac{d_2}{d_1}-1\right)^2 + O(\vartheta^3), \qquad (30.62)$$